A Lagrangian probability-density-function model for turbulent particle-laden channel flow in the dense regime

Alessio Innocenti[a)]

LaMMA Consortium, Environmental Modelling and Monitoring Laboratory for the Sustainable Development, Florence, Italy

Rodney O. Fox

Department of Chemical and Biological Engineering, 618 Bissell Road, Iowa State University, Ames, IA 50011-1098, USA

Sergio Chibbaro

Sorbonne University, UPMC Univ Paris 06, CNRS, UMR 7190, Institut Jean Le Rond d'Alembert, F-75005 Paris, France

Modeling particle-laden turbulent flows at high volume fractions requires accounting for the coupling between phases. The latter is often a sensitive point, and proper closure of the exchange and production terms due to the presence of particles is not straightforward. In the present work, a Lagrangian probability-density-function (PDF) model developed for homogeneous cluster-induced turbulence is extended to a channel flow. The key features are consistent two-way coupling and the decomposition of the particle velocity into spatially correlated and uncorrelated components, which is crucial for dense flows, and which allows to deal with collisions from a statistical point of view. A numerical scheme for the coupled solution of the stochastic differential equations for the particles and a Reynolds-stress model for the fluid is developed. Tests with tracer particles without two-way coupling are done to assess the validity and the consistency of the numerical scheme. Finally, two sets of numerical simulations with particles with different diameters in a turbulent channel flow at a shear Reynolds of $Re_\tau = 300$ are reported. The effect of two-way coupling by varying the mass loading of the dispersed phase in the mass-loading range $\varphi = 0$–2 is analyzed, and the results are compared to previous Eulerian–Lagrangian (EL) and Eulerian–Eulerian (EE) direct-numerical simulation (DNS) studies. Mean velocities and turbulent kinetic energy show good agreement with DNS, especially regarding the trend with respect to mass loading. Consistent with prior work, increased mass loading causes a drastic reduction of turbulent kinetic energy in the range $\varphi = 0$–2.

---

[a])Electronic mail: a.innocenti@lamma.toscana.it

I. INTRODUCTION

Particle-laden turbulent flows are present in a number of industrial and geophysical applications and their study has a long history in the literature. Depending on the volume fraction of the particle phase within the flow, different regimes have been identified with totally different mechanisms of energy production and transfer between the phases[1,2]. Several pioneering works[3–5] have investigated the so-called dilute regime, where interphase coupling can be null or negligible, and the majority of the fluid-phase turbulence is generated by mean shear. In this regime, the particles exhibit several features caused by their interaction with turbulent structures. For instance, they tend to group together in particular regions of the flow, depending on their inertia, and to form clusters[5]. Increasing the volume fraction, the effect of the particles on the fluid phase cannot be neglected anymore and at some point collisions start to be also important[6,7]. At sufficiently high mass loading ($\varphi = \rho_p \alpha_p / (\rho_f \alpha_f) \gtrsim 1$), recent works using both Eulerian–Lagrangian (EL) and Eulerian–Eulerian (EE) methods[8–10] have shown that even for homogeneous conditions, spatial fluctuations of particle clusters can generate turbulence in a resting fluid due to the effect of gravity. Under these conditions, turbulence is mainly fed by the mean-slip velocity of the clusters instead of the classical mean-shear production. Thus, the primary source of turbulence production is a term proportional to the drift velocity and mean slip between the phases. At intermediate mass loading of order unity, it has been found[1,11] that particles tend to reduce the turbulent kinetic energy of the carrier phase, and relaminarization of the flow is even possible. Inhomogeneous flows are particularly interesting and challenging, because they show important preferential concentration in certain regions, notably near to the walls in a channel. In this case, it may be found that significant effects due to coupling and collisions cannot be neglected locally even in those cases for which the average volume fraction would indicate a dilute regime.

The most widely used numerical approach for particle-laden flows is EL point-particle simulations[12]. With this approach, the continuous fluid phase is described by means of a direct-numerical simulation (DNS) or with a turbulence model (e.g., Reynolds-averaged (RA) equations, large-eddy simulations (LES)), and the dispersed particle phase is tracked with a Lagrangian point of view[13,14]. This type of approach offers an extremely good approximation whenever particles are very small compared to the smallest turbulence length

3

scales. Otherwise, the particle size should be taken into account explicitly through particle-resolved simulations[15,16]. The coupling of fluid-phase turbulence models with the Lagrangian equations of particle motion has been shown to suffer from several drawbacks, e.g., a wrong estimation of particle clustering and concentration, because of the lack of information due to the reduced level of description[17–19]. Several works have shown the possibility of partially reconstructing the fluid-phase fluctuations by means of a stochastic model in the equation of particle motion[20–22] for dilute flows.

From an historical perspective, stochastic or probability-density-function (PDF) methods have been developed in turbulence since the 1960s[23], and key advances towards the modern modeling approach were carried out by Ted O'Brien[24–30]. PDF methods are useful because of the exact treatment of nonlinear terms local in variable space[31–33]. They are widely used in reactive flows[34], and have been extended to particle-laden flows more recently[20,35–37].

Our recent work has extended the possibility to use this class of Lagrangian models with high mass loading[38], where collisions are considered from a statistical point of view. Namely a stochastic particle model has been developed for the case of homogeneous fully developed cluster-induced turbulence (CIT) based on the exact mesoscopic equations derived from the kinetic theory of collisional fluid–particle flows. In the present work, we test this model for an inhomogeneous application, i.e., a channel flow, comparing our results with a EL-DNS[1], a EE-DNS[2], and a Reynolds-stress model[39], with a mass loading in the range $0 \leq \varphi \leq 2$, therefore from dilute to moderately dense flows. It is worth remarking that for the lower mass loading tested, simpler versions of the particle model[20] with only two-way coupling and without particle collisions, could equally be valid. However, it has been shown[38] that the present model developed for dense flows is consistent with the two-way model and gives correct results also in the dilute regime. Therefore, the analysis of such a model may give insights into the physical mechanisms at play in the different regimes.

In contrast to homogeneous CIT where the agreement between EE and EL approaches is quite satisfactory[9,10] for all Stokes numbers, a recent work[2] found that the EE-DNS breaks down for high-Stokes-number particles at low volume fractions when compared to EL-DNS for vertical channel flows. Similar issues are observed with the EE Reynolds-stress model (RSM) of Baker *et al.*[39] where qualitative agreement is obtained only for low-Stokes-number particles.

Our goal is to try to improve on that work by formulating a stochastic model for dense

flows including the fluid seen by particles, which is modeled through a crude correlation in the EE RSM that is not justified near the channel walls. The stochastic model starts at a more fundamental basic that should allow for improvements using physics-based modeling. Thus, our objective here is to assess the particle Lagrangian model developed for dense flows[38] at high mass loading and different Stokes numbers, which has been already assessed for homogeneous CIT. In particular, we test whether the Lagrangian formulation is able to capture better the transition of the flow that occurs when increasing the mass loading from zero to values above unity as compared to the EE RSM[39] with comparable turbulence closures. Yet, it remains out of the scope of the present work to provide a complete calibration of the model that could lead to a more accurate comparison with DNS. The purpose of this work is to appraise the Lagrangian stochastic model's capability to describe inhomogeneous flows, and in this framework we stick with the model parameters previously validated. This analysis is already a valuable contribution since in this approach information is available that is not in EE RANS models.

The remainder of this work is organized as follows. In section II, we summarize the Lagrangian model equation for the channel flow case. In section III, the flow and geometric parameters of the vertical channel flow are described. In section IV, a new numerical scheme is derived for the solution of coupled stochastic differential equations (SDE). In section V, we present results for tracer and inertial particles with mass loading up to $\varphi = 2$, and compare them to prior work.

II. LAGRANGIAN PDF MODEL FOR VERTICAL CHANNEL FLOW

Here we provide an overview of the model equations for dense fluid–particle flows derived in a recent work[38], and adapted to a vertical channel flow. We consider a channel of width W, with the span-wise direction denoted by x, the wall-normal direction by y ($0 \leq y \leq W$), and the vertical direction by z. All time-averaged statistical quantities depend only on the wall-normal direction, y. The fluid–particle model consists in a set of Reynolds-average (RA) equations for the fluid phase, and a set of Lagrangian stochastic equations for the particle phase with two-way coupling. In the RA fluid-phase model equations, the only relevant quantities for channel flow are the following: $\langle U_{f,z} \rangle$ (mean vertical velocity), $\langle u_{f,x} u_{f,x} \rangle$, $\langle u_{f,y} u_{f,y} \rangle$, $\langle u_{f,z} u_{f,z} \rangle$, $\langle u_{f,y} u_{f,z} \rangle$ (Reynolds-stress tensor). In addition, a transport equation

for the fluid-phase dissipation ε_f has to be included to close the model. On the other hand, the modeled Lagrangian quantities are y_p (particle wall-normal position), $\delta\mathbf{v}_p$, $\mathbf{U}_p$ and $\mathbf{U}_s$, which are, respectively, the uncorrelated velocity, the correlated in space particle velocity, and the fluid velocity seen by particles. The latter is the most natural choice in Lagrangian two-phase stochastic models, since it represents the fluid velocity at the particle position, i.e., sampled along particle trajectories. It takes into account the fact that solid particles do not follow fluid–particle trajectories due to particle inertia. It is generally used also in dilute models, though without the terms responsible for two-way coupling, and it is worth remarking that in the limit of vanishing particle inertia it should retrieve the Lagrangian fluid velocity.

The Lagrangian particle velocity V_p has been split into two components U_p and δv_p via a coarse-graining approach on the kinetic equation. This procedure was initially proposed for dilute two-phase turbulent flows[40] and for collisional dense flows[41], both in an Eulerian framework, and formalized in a Lagrangian sense[38]. The coarse-graining operation consists in filtering the microscale total particle velocity V_p to obtain a filtered mesoscale component U_p that represents the correlated part of the microscale velocity, and a residual uncorrelated component δv_p that has zero mean and is uncorrelated with U_p. Also, for the dispersed phase, an additional dissipation transport equation for ε_p is necessary to close the model. The stream-wise and span-wise components of the particle position are not relevant since the channel is periodic in those directions. Particle statistics are evaluated over slabs parallel to the channel walls.

For the unfamiliar reader, stochastic Lagrangian models are the Lagrangian counterpart of Eulerian RA models, though with fewer unclosed terms. Each statistical Lagrangian particle represents a fluid/particle realization and, with a sufficient number of samples, RA quantities can be reconstructed from local spatial averaging. From a formal point of view, fluid- and particle-phase RA transport equations can be derived from the stochastic Lagrangian ones (in single-phase turbulence[33] , in two-phase turbulence[42] , and for the present model[38]); however, some transport terms would remain unclosed and a direct solution of the RA equations would not be possible without further modeling. This is one of the advantages of sticking to the Lagrangian description, together with the fact that some modeling assumptions are more natural and straightforward from the particle point of view.

A. Stochastic model for particle phase

We review here the set of SDEs for the particle phase proposed in Innocenti *et al.*[38], expressed for an inhomogeneous flow. The Lagrangian particle position in the wall-normal direction is

$$dy_p = V_{p,y}\,dt = (U_{p,y} + \delta v_{p,y})\,dt \tag{1}$$

where $\mathbf{V}_p$ is the particle velocity. As previously explained[38], following previous Eulerian models for dilute[40] and dense[8] flows, the particle velocity is decomposed into a spatially correlated part $\mathbf{U}_p$, and a uncorrelated residual $\delta \mathbf{v}_p$, derived from a coarse-graining/filtering approach. The former is governed by

$$dU_{p,i} = \frac{1}{\tau_p}(U_{s,i} - U_{p,i})\,dt + g_i\,dt - \frac{1}{\langle \alpha_p \rangle}\frac{\partial \langle \alpha_p \rangle \langle P_{ij} \rangle}{\partial x_j} + \delta v_{p,j}\frac{\partial \langle U_{p,i} \rangle}{\partial x_j}\,dt$$
$$- \frac{1}{T_{Lp}}(U_{p,i} - \langle U_{p,i} \rangle)\,dt + \sqrt{C_p \varepsilon_p}\,dW_{p,i}. \tag{2}$$

The first term of the RHS of (2) is the drag force exerted by the fluid on the particle. $\mathbf{U}_s$ is the fluid velocity seen by the particle, i.e. at the particle position. $\mathbf{U}_p$ is the correlated component of the particle velocity. $\tau_p = \rho_p d_p^2/(18\rho_f \nu_f)$ is the particle relaxation time (hereinafter taken as a constant). d_p is the particle diameter, and ν_f the kinematic viscosity of the fluid. This drag force is the only contribution accounting for the effect of the fluid phase on particles, which is justified by the large density ratio limit $\rho_p/\rho_f \gg 1$. The second term is the gravitational acceleration, $\mathbf{g} = [0,\ 0,\ g]^T$. The third term is a pressure term with $\langle \alpha_p \rangle$ being the particle-phase volume fraction and $\langle P_{ij} \rangle = \langle \delta v_{p,i} \delta v_{p,j} \rangle$ the particle-phase pressure tensor. The brackets $\langle \cdot \rangle$ denote phase-specific Reynolds average, i.e., weighted with the respective volume fraction. Therefore they stand as an abbreviation of $\langle (\cdot) \rangle_p = \langle \alpha_p (\cdot) \rangle / \langle \alpha_p \rangle$ when averaging particle-phase quantities, and of $\langle (\cdot) \rangle_f = \langle \alpha_f (\cdot) \rangle / \langle \alpha_f \rangle$ when averaging fluid-phase quantities. It is worth noting that in a Lagrangian approach, when doing an ensemble average of particle quantities over a computational cell, we are intrinsically weighting with the volume fraction.

The fourth term in (2) comes directly in closed form from the coarse-graining procedure[38] and is a transport term for the filtered particle velocity $\mathbf{U}_p$ due to the uncorrelated part $\delta \mathbf{v}_p$, and has its counterpart in the Lagrangian transport equation of the uncorrelated particle velocity $\delta \mathbf{v}_p$ (Equation (5)). In practice, since the two particle velocity components are uncorrelated and $\langle \delta \mathbf{v}_p \rangle = 0$, it gives no contribution either in the first-order moment transport

7

equation for $d\langle \mathbf{U}_p \rangle$ nor in the second-order one for $d\langle \mathbf{u}_p \cdot \mathbf{u}_p \rangle$. However, it is important to balance the corresponding term in (5) when the total particle velocity $\mathbf{V}_p$ is evaluated as the summation of the two components, and therefore to avoid spurious drift.

The fifth term in (2) is a relaxation to equilibrium term, which brings the instantaneous particle velocity $\mathbf{U}_p$ towards its average value on the Lagrangian integral time scale T_{Lp}:

$$T_{Lp} = \frac{2}{\left(1 + \frac{3}{2}C_{0p} + f_s\right)} \frac{k_p}{\varepsilon_p}. \tag{3}$$

$k_p = \frac{1}{2}\langle \mathbf{u}_p \cdot \mathbf{u}_p \rangle$ is the fluctuating kinetic energy of the correlated particle velocity, and ε_p the particle-phase dissipation rate. In particular, the following relation holds for the fluctuating energy partitioning: $\kappa_p = k_p + \frac{3}{2}\langle \Theta_p \rangle$, where $\kappa_p = \frac{1}{2}\langle \mathbf{v}_p \cdot \mathbf{v}_p \rangle$ is the total particle-phase fluctuating energy, $k_p = \frac{1}{2}\langle \mathbf{u}_p \cdot \mathbf{u}_p \rangle$ is the particle-phase turbulent kinetic energy, and $\langle \Theta_p \rangle = \frac{1}{3}\langle \delta\mathbf{v}_p \cdot \delta\mathbf{v}_p \rangle$ is the particle-phase granular temperature. $\mathbf{v}_p$ and $\mathbf{u}_p$ are the fluctuations arising from the Reynolds decomposition of $\mathbf{V}_p$ and $\mathbf{U}_p$, respectively.

The last term in (2) is an isotropic diffusion term, in which the constant C_p is related to C_{0p} by the relation

$$C_p = C_{0p} + \frac{2}{3}f_s, \tag{4}$$

in order to obtain the correct correlation at the Reynolds-stress level. Finally, $dW_{p,i}$ is a Wiener stochastic process. It is worth remarking that the present model lies at the mesoscale and reintroduces the turbulent fluctuations of the small-scale particle velocity through the last two terms. This is different from classical two-phase dilute stochastic models where the particle-phase turbulence due to collisions is not considered, assuming intrinsically that $\mathbf{V}_p = \mathbf{U}_p$ and that the particle acceleration $d\mathbf{V}_p$ is driven only by fluid drag and gravity. Therefore, with the present model, the combined effect of the last two terms in (2) is analogous to the drift and diffusion terms used in the generalized Langevin model[33] for single-phase turbulent flows. From a modeling point of view this type of closure yields, in the transport equation of the particle-phase Reynolds stresses, a redistribution of particle turbulent energy between the Reynolds stresses $\mathcal{R}_p$, and a sink (dissipation) ϵ_p towards the granular component, analogously to the Rotta model for single-phase turbulent flows[38].

The uncorrelated residual particle velocity is modeled through an additional Lagrangian stochastic equation attached to the same "statistical" particle. It retains mainly the effect of spatial decorrelation due to inter-particle collisions and particle inertia. In particular, the

exact form of $d\delta\mathbf{v}_p$ coming from the coarse-graining procedure as the difference between the total and the filtered components is unclosed and requires a model. Such a closure[38] has been guessed to obtain the correct transport equation for the particle granular temperature $\langle\Theta_p\rangle = \frac{1}{3}\langle\delta\mathbf{v}_p \cdot \delta\mathbf{v}_p\rangle$, and resulted in the following model:

$$d\,\delta v_{p,i} = -\frac{1}{\tau_p}\delta v_{p,i}\,dt + \frac{1}{\langle\alpha_p\rangle}\frac{\partial\langle\alpha_p\rangle\langle P_{ij}\rangle}{\partial x_j} - \delta v_{p,j}\frac{\partial\langle U_{p,i}\rangle}{\partial x_j}\,dt + B_{\delta,ij}\,dW_{\delta,j}$$
$$-\frac{(1+e)(3-e)}{4\tau_c}\delta v_{p,i}\,dt + \sqrt{\frac{1}{2\tau_c}(1+e)^2\langle\Theta_p\rangle}\,dW_{c,i}. \quad (5)$$

The first term is the residual uncorrelated part of the drag term, evaluated from the difference between the total and the correlated particle velocities. The next two terms are the same as in (2) with opposite sign, as they need to vanish in order to obtain the correct average particle equation. The diffusion coefficient in the fourth term has instead to be different, as it represents the fluctuating component. In particular B_δ is a diffusion matrix, whose expression will be given in the following, and dW_δ is a Wiener stochastic process uncorrelated with dW_p.

The last two terms have been introduced to take into account collisions, where e is a restitution coefficient and dW_c is another Wiener process. The collision deterministic term is driven by a characteristic collision time scale τ_c:

$$\tau_c = \frac{\sqrt{\pi}d_p}{6C_c\langle\alpha_p\rangle\langle\Theta_p\rangle^{1/2}}, \quad (6)$$

where C_c is a model parameter[43].

The diffusion matrix $B_{\delta,ij}$ (shown in Appendix A) is formulated in order to obtain the correct closure for second-order moments of the uncorrelated velocity[38] $\langle\delta v_{p,i}\delta v_{p,j}\rangle$, resulting in a dissipation tensor in the transport equation of $\langle\delta v_{p,i}\delta v_{p,j}\rangle$ as follows:

$$\boldsymbol{\epsilon}_p = \varepsilon_p\left[f_s\frac{\langle\mathbf{u}_p \otimes \mathbf{u}_p\rangle}{k_p} + (1-f_s)\frac{2}{3}\mathbf{I}\right] \quad (7)$$

where ε_p is one-half the trace of $\boldsymbol{\epsilon}_p$, and $0 \leq f_s \leq 1$ is a parameter tuning the anisotropy. In particular, with the present models for $\mathbf{U}_p$ and $\delta\mathbf{v}_p$, it can be shown that an exchange of energy is obtained from the correlated turbulent particle-phase energy k_p towards the granular temperature $\langle\Theta_p\rangle$, through a sink (dissipation) $-\boldsymbol{\epsilon}_p$ and a source $+\boldsymbol{\epsilon}_p$ in the respective RA transport equations. Thanks to the closure proposed in Innocenti *et al.*[38], such transfer of energy takes into account the anisotropy of the flow, reflecting the physical mechanism

9

of transfer due to the correlation between particle velocity gradients[8], as for single-phase turbulence.

The dissipation rate associated with a particle is modeled through a deterministic Eulerian equation in analogy to single-phase flows:

$$\frac{d\varepsilon_p}{dt} = (C_{\epsilon 1p}\mathcal{P}_{Sp} - C_{\epsilon 2p}\varepsilon_p)\frac{\varepsilon_p}{k_p} + \frac{C_{3p}}{\tau_p}\left(\frac{k_{fp}}{k_{f@p}}\varepsilon_f - \beta_p\,\varepsilon_p\right) \tag{8}$$

where $C_{\epsilon 1p}$, $C_{\epsilon 2p}$, C_{3p} and β_p are model parameters. k_{fp} and $k_{f@p}$ are one half the trace of the second-order correlations between fluid and particle and the fluid with itself at the particle position, respectively. They are defined as $k_{fp} = \frac{1}{2}\langle \mathbf{u}_s \cdot \mathbf{u}_p \rangle$, $k_{f@p} = \frac{1}{2}\langle (\mathbf{U}_s - \langle \mathbf{U}_f\rangle) \cdot (\mathbf{U}_s - \langle \mathbf{U}_f\rangle)\rangle$. Equation (8) has been derived empirically in order to obtain the correct decay in isotropic decaying turbulence and homogeneous shear turbulence with varying particle inertia. It is worth noting that this expression is different from that proposed by Fox *et al.*[41] because additional information is available in the Lagrangian model (e.g., k_{fp} and $k_{f@p}$) that is unavailable in the EE model. Nevertheless, the drag-exchange term in (8) must be modeled in either formulation. Thus, other closures may be required to obtain the correct behavior of the ratio k_p/k_f[41].

B. Stochastic model for fluid seen by particles

The fluid velocity seen by the particles is a key variable in two-phase models and its Lagrangian model offers one of the main advantages with respect to Eulerian RA models[9,39,43], where $\langle \mathbf{U}_s \rangle$ is usually guessed as some empirical function of $\langle \mathbf{U}_f \rangle$. In the first works[20,35,42], a Lagrangian stochastic model for $\mathbf{U}_s$ has been developed for dilute flows starting from the generalized Langevin model for the single-phase turbulent fluid velocity $\mathbf{U}_f$[33], and accounting for the fact that inertial particles deviate from fluid trajectories by modifying mainly the Lagrangian fluid time scale appearing in the drift term and indirectly in the diffusion coefficient of the fluid model, transforming therefore the variable from $\mathbf{U}_f$ to $\mathbf{U}_s$.

The present model for the fluid velocity seen by the particles is in some sense a generalization of the model for dilute flows[20,42] to dense flows. In particular, here we use a modified pressure gradient weighted by the fluid-phase volume fraction, and a different diffusion coefficient, which takes into account a possible velocity difference between the fluid average

velocity, $\langle \mathbf{U}_f \rangle$, and the mean fluid velocity seen by particles, $\langle \mathbf{U}_s \rangle$:

$$
dU_{s,i}(t) = -\frac{\langle \alpha_f \rangle}{\rho_f}\frac{\partial \langle p_f \rangle}{\partial x_i}\, dt + G_{i,j}(U_{s,j} - \langle U_{f,j} \rangle)\, dt - \frac{\varphi}{\tau_p}(U_{s,i} - U_{p,i})\, dt + g_i\, dt
$$

$$
+ \left[\varepsilon_f \left(C_{0f} b_i \frac{\tilde{k}_f}{k_f} + \frac{2}{3}\left(b_i \frac{\tilde{k}_f}{k_f} - 1 \right) \right) + \frac{2\varphi}{\tau_p}(\langle U_{p,i} \rangle - \langle U_{s,i} \rangle)(\langle U_{s,i} \rangle - \langle U_{f,i} \rangle) \right.
$$

$$
\left. -2\frac{\langle \alpha_p \rangle}{\rho_f}\frac{\partial \langle p_f \rangle}{\partial x_i}(\langle U_{s,i} \rangle - \langle U_{f,i} \rangle) + \frac{2}{3}C_{2f}\mathcal{P}_{Sfs} \right]^{1/2} dW_{s,i}. \quad (9)
$$

The first term of the RHS is the pressure gradient weighted by the fluid-phase volume fraction. The second term is a return to equilibrium term, where the coefficient

$$
G_{ij} = -\frac{1}{T_{L,i}^*}\delta_{ij} + G_{ij}^a. \quad (10)
$$

$T_{L,i}^*$ is a modified fluid Lagrangian time-scale taking into account the anisotropy of the flow and particle inertia, defined by

$$
T_{L,i}^* = \frac{T_{Lf}}{\sqrt{1 + \zeta_i \beta^2 \frac{3|\langle \mathbf{U}_r \rangle|^2}{2k_f}}}, \quad T_{Lf} = \frac{2}{\left(1 + \frac{3}{2}C_{0f}\right)}\frac{k_f}{\varepsilon_f}. \quad (11)
$$

$\zeta_1 = 1$ in the mean-drift direction and $\zeta_{2,3} = 4$ in the cross directions. $\beta = T_{Lf}/T_{Ef}$ is the ratio of the Lagrangian and the Eulerian timescales, and $\mathbf{U}_r = \mathbf{U}_p - \mathbf{U}_s$ is the relative velocity. k_f and ε_f are the fluid turbulent kinetic energy and dissipation. $\mathbf{G}^a$ is a traceless matrix to be added to generalize the model[38]. In particular, for a correspondence with the isotropization-of-production (IP) model of Launder–Reece–Rodi[44] (LRR-IP), it should be

$$
G_{ij}^a = C_{2f}\frac{\partial \langle U_{f,i} \rangle}{\partial x_j}, \quad (12)
$$

with C_{2f} being the IP constant. The value of the model constant C_{0f} used in the Lagrangian time-scale is established by the relation[45]:

$$
C_{0f} = \frac{2}{3}\left(C_{Rf} - 1 \right), \quad (13)
$$

where C_{Rf} is the Rotta constant.

The third term on the right-hand side of (9) accounts for two-way coupling. Therefore, it is represented by the opposite of the drag force, φ being the mean mass loading, defined as $\varphi = \frac{\rho_p \langle \alpha_p \rangle}{\rho_f \langle \alpha_f \rangle}$. The fourth term is gravity, and the last term is a stochastic diffusion process extended to dense flows in which $b_i = T_{Lf}/T_{L,i}^*$,

$$
\tilde{k}_f = \frac{3}{2}\frac{\sum_{i=1}^{3} b_i \langle (U_{s,i} - \langle U_{f,i} \rangle)^2 \rangle}{\sum_{i=1}^{3} b_i}, \quad (14)
$$

and $\mathcal{P}_{Sfs}$ is one-half the trace of the tensor

$$\mathcal{P}_{Sfs} = -\left(\langle(\mathbf{U_s} - \langle\mathbf{U}_f\rangle) \otimes (\mathbf{U_s} - \langle\mathbf{U}_f\rangle)\rangle \cdot \nabla\langle\mathbf{U}_f\rangle\right)^\dagger . \tag{15}$$

The Wiener process dW_s is uncorrelated with those present in the particle equations.

For the sake of brevity, we do not report here the corresponding Eulerian transport equations for $\langle\mathbf{U_s}\rangle$, $\langle\mathbf{U_p}\rangle$ and the related Reynolds stresses, which are analyzed in detail in Innocenti et al.[38]. Here, we just stress the main differences with respect to single-phase turbulence models such as the simplified Langevin model (SLM)[33]:

$$dU_{f,i}(t) = -\frac{1}{\rho_f}\frac{\partial\langle p_f\rangle}{\partial x_i}\,dt + \frac{1}{T_L}(U_{f,i} - \langle U_{f,i}\rangle)\,dt + (C_0\varepsilon_f)^{1/2}dW_{f,i}. \tag{16}$$

Comparing (9) to the SLM, (i) the pressure gradient is weighted with the fluid-phase volume fraction, (ii) the Lagrangian time-scale in the return-to-equilibrium drift term is modified to take into account particle inertia and anisotropy with the expression proposed previously[20,35], (iii) the third term is the opposite of fluid drag force and represents the direct effect of particles on fluid, (iv) the fourth term is gravity which is relevant in two-phase flows with different densities and is included in the pressure gradient in single-phase flows, and (v) the last term is a diffusion coefficient corresponding to the last term in (16) with several modifications in order to take into account the differences in the drift terms and to ensure a consistent closure for the second-order moments RA transport equations for $\langle\mathbf{u_s} \otimes \mathbf{u_s}\rangle$.

To summarize, the particle phase and fluid seen are described by the following system of SDEs:

$$d\mathbf{Z}_p = \mathbf{A}\,dt + [B]\,d\mathbf{W}, \tag{17}$$

where $\mathbf{A}$ is the drift term, and

$$\mathbf{Z}_p = \begin{pmatrix} \mathbf{U}_p \\ \delta\mathbf{v}_p \\ \mathbf{U}_s \end{pmatrix} \qquad [B] = \begin{bmatrix} C[I] & 0 & 0 & 0 \\ 0 & [B_\delta] & K[I] & 0 \\ 0 & 0 & 0 & [B_s] \end{bmatrix} \qquad d\mathbf{W} = \begin{pmatrix} d\mathbf{W}_p \\ d\mathbf{W}_\delta \\ d\mathbf{W}_c \\ d\mathbf{W}_s \end{pmatrix}. \tag{18}$$

$C = \sqrt{C_p\varepsilon_p}$ is the diagonal diffusion coefficient in the equation for the correlated velocity. $K = \sqrt{1/(2\tau_c)(1 + e^2)\langle\Theta_p\rangle}$ is the diagonal diffusion coefficient for the collisions in the uncorrelated-velocity equation. B_s is the diffusion coefficient in the fluid-velocity-seen-by-particles equation.

C. Fluid-phase turbulence model

Hereinafter, we assume that $\langle \alpha_f \rangle$ is time independent. However, as shown in previous works[39], this need not be the case at high mass loading due to the one-dimensional nature of CIT. The steady-state transport of the RA fluid-phase volume fraction $\langle \alpha_f \rangle$ reduces to the wall-normal component

$$\frac{\partial \langle \alpha_f \rangle \langle U_{f,y} \rangle}{\partial y} = 0. \tag{19}$$

Since the wall-normal velocity is null at the walls, this expression yields $\langle U_{f,y} \rangle (y) = 0$.

The only non-zero components of the fluid-phase momentum equation are given by

$$0 = -\frac{1}{\rho_f} \frac{\partial \langle p_f \rangle}{\partial y} - \frac{1}{\langle \alpha_f \rangle} \frac{\partial \langle \alpha_f \rangle \langle u_{f,y} u_{f,y} \rangle}{\partial y} - \frac{\varphi}{\tau_p} \langle U_{s,y} \rangle, \tag{20}$$

$$\frac{\partial \langle U_{f,z} \rangle}{\partial t} = -\frac{1}{\rho_f} \frac{\partial \langle p_f \rangle}{\partial z} - \frac{1}{\langle \alpha_f \rangle} \frac{\partial \langle \alpha_f \rangle \langle u_{f,y} u_{f,z} \rangle}{\partial y} + \nu_f \frac{\partial^2 \langle U_{f,z} \rangle}{\partial y^2} - g + \frac{\varphi}{\tau_p} (\langle U_{p,z} \rangle - \langle U_{s,z} \rangle), \tag{21}$$

where $\varphi(y) = \rho_p \langle \alpha_p \rangle / (\rho_f \langle \alpha_f \rangle)$ is the RA mass loading. From (20), the pressure gradient in the y direction can be determined for use in the Lagrangian equation for U_s. Here we seek a steady-state solution where the left-hand side of (21) is null.

There are four non-zero components of the Reynolds-stress tensor: xx, yy, zz, yz, which are governed by

$$\frac{\partial \langle u_{f,x} u_{f,x} \rangle}{\partial t} = \mathcal{R}_{f,xx} - \epsilon_{f,xx} + \mathcal{DE}_{f,xx} + \frac{1}{\langle \alpha_f \rangle} \frac{\partial}{\partial y} \left(\langle \alpha_f \rangle (\nu_{ft} + \nu_f) \frac{\partial \langle u_{f,x} u_{f,x} \rangle}{\partial y} \right), \tag{22}$$

$$\frac{\partial \langle u_{f,y} u_{f,y} \rangle}{\partial t} = \mathcal{R}_{f,yy} - \epsilon_{f,yy} + \mathcal{DE}_{f,yy} + \frac{1}{\langle \alpha_f \rangle} \frac{\partial}{\partial y} \left(\langle \alpha_f \rangle (\nu_{ft} + \nu_f) \frac{\partial \langle u_{f,y} u_{f,y} \rangle}{\partial y} \right), \tag{23}$$

$$\frac{\partial \langle u_{f,z} u_{f,z} \rangle}{\partial t} = \mathcal{R}_{f,zz} - \epsilon_{f,zz} - 2 \langle u_{f,y} u_{f,z} \rangle \frac{\partial \langle U_{f,z} \rangle}{\partial y} + \mathcal{DE}_{f,zz} + \mathcal{DP}_{f,zz}$$
$$+ \frac{1}{\langle \alpha_f \rangle} \frac{\partial}{\partial y} \left(\langle \alpha_f \rangle (\nu_{ft} + \nu_f) \frac{\partial \langle u_{f,z} u_{f,z} \rangle}{\partial y} \right), \tag{24}$$

$$\frac{\partial \langle u_{f,y} u_{f,z} \rangle}{\partial t} = \mathcal{R}_{f,yz} - \epsilon_{f,yz} - \langle u_{f,y} u_{f,y} \rangle \frac{\partial \langle U_{f,z} \rangle}{\partial y} + \mathcal{DE}_{f,yz}$$
$$+ \frac{1}{\langle \alpha_f \rangle} \frac{\partial}{\partial y} \left(\langle \alpha_f \rangle (\nu_{ft} + \nu_f) \frac{\partial \langle u_{f,y} u_{f,z} \rangle}{\partial y} \right). \tag{25}$$

$\mathcal{DP}_{f,ij}$ and $\mathcal{DE}_{ij}$ are the drag-production and drag-exchange tensors:

$$\mathcal{DP}_{f,ij} = \frac{2\varphi}{\tau_p} (\langle U_{s,z} \rangle - \langle U_{f,z} \rangle)(\langle U_{p,z} \rangle - \langle U_{f,z} \rangle) \delta_{iz} \delta_{jz}, \tag{26}$$

$$\mathcal{DE}_{f,ij} = \frac{\varphi}{\tau_p} (\langle u_{s,i} u_{p,j} \rangle + \langle u_{p,i} u_{s,j} \rangle - 2 \langle (U_{s,i} - \langle U_{f,i} \rangle)(U_{s,j} - \langle U_{f,j} \rangle) \rangle). \tag{27}$$

For the vertical channel flow, $\mathcal{DP}_{f,zz}$ is the only nonzero drag-production term and arises because the formation of clusters leads to $\langle U_{s,z} \rangle \neq \langle U_{f,z} \rangle$. It is worth noting that in the EE Reynolds-stress model of Baker et al.[39], a closure must be provided for $\langle U_{s,z} \rangle$, which is the major source of mismatch with EL-DNS. In contrast, quantities involving U_p and U_s are available from the Lagrangian particle solver.

The redistribution tensor $\mathcal{R}_{f,ij}$ is modeled using the Rotta model:

$$\mathcal{R}_{f,ij} = -C_R \frac{\varepsilon_f}{k_f} \left(\langle u_{f,i} u_{f,j} \rangle - \frac{2}{3} k_f \delta_{ij} \right) - C_{2f} \left(\mathcal{P}_{Sf,ij} - \frac{2}{3} \mathcal{P}_{Sf} \delta_{ij} \right) \tag{28}$$

with mean-shear-production tensor

$$\mathcal{P}_{Sf,ij} = -\langle u_{f,i} u_{f,k} \rangle \frac{\partial \langle U_{f,j} \rangle}{\partial x_k} - \langle u_{f,j} u_{f,k} \rangle \frac{\partial \langle U_{f,i} \rangle}{\partial x_k}; \tag{29}$$

and $\mathcal{P}_{Sf} = \frac{1}{2} trace(\boldsymbol{P}_{Sf})$. For the vertical channel flow, only $\frac{\partial \langle U_{f,z} \rangle}{\partial y}$ is nonzero.

The wall-normal transport terms for the Reynolds-stress tensors are closed using a gradient-diffusion model with the following turbulent viscosity:

$$\nu_{ft} = C_s \frac{k_f}{\varepsilon_f} \langle u_{f,y} u_{f,y} \rangle. \tag{30}$$

The standard value for the model constant is $C_s = 0.22$. At high mass loading in a vertical channel, $|\langle u_{f,y} u_{f,z} \rangle| < \langle u_{f,y} u_{f,y} \rangle \ll \langle u_{f,z} u_{f,z} \rangle$ (i.e., the turbulence is nearly one-dimensional[33]) and, hence, wall-normal turbulent transport is relatively small compared to single-phase flow[2]. Since wall-normal turbulent transport is the main stabilization mechanism in turbulent channel flows, this situation can result in time-dependent solutions as the mass loading increases[39].

An anisotropic form of the dissipation tensor has been chosen, including a low-Reynolds model when the wall is approached:

$$\epsilon_{f,ij} = f_s \frac{\langle u_{f,i} u_{f,j} \rangle}{k_f} + (1 - f_s) \frac{2}{3} \varepsilon_f \delta_{ij} \tag{31}$$

with

$$f_s = \exp\left[-\left(\frac{Re_L}{150} \right)^2 \right] \tag{32}$$

and $Re_L = k_f^2/(\nu_f \varepsilon_f)$. To completely close the above set of equations describing the fluid phase, we still need an equation for the fluid-phase turbulent dissipation rate:

$$\frac{\partial \varepsilon_f}{\partial t} = (C_{\epsilon 1f} \mathcal{P}_{Sf} - C_{\epsilon 2f} \varepsilon_f) \frac{\varepsilon_f}{k_f} + C_{3f} \frac{\varphi}{\tau_p} \left(\frac{k_{fp}}{k_{f@p}} \varepsilon_p - \beta_f \varepsilon_f \right) + C_4 \frac{\varepsilon_p}{k_p} \mathcal{DP}$$
$$+ \frac{1}{\langle \alpha_f \rangle} \frac{\partial}{\partial y} \left[\langle \alpha_f \rangle \left(\frac{\nu_{ft}}{\sigma_\epsilon} + \nu_f \right) \frac{\partial \varepsilon_f}{\partial y} \right] \tag{33}$$

14

where $C_{\epsilon 1f}$, $C_{\epsilon 2f}$, C_{3f}, β_f and C_4 are model constants, and $\mathcal{DP}$ is one half the trace of $\mathcal{DP}_{f,ij}$. It should be noted that (33) has some additional terms with respect to single-phase turbulent dissipation models. In particular the second and third terms on the RHS are due to the coupling with the particle phase and are modeled in accordance with (8) to obtain the correct decay regimes in some reference cases (isotropic turbulence, homogeneous shear, homogeneous CIT)[38]. To better capture the near-wall behavior, the fluid-phase turbulence integral time scale is defined as $T_f = \max(k_f/\varepsilon_f, 6\sqrt{\nu_f/\varepsilon_f})$ in the RA equations. Let us note that the time-scale used for the drag-production term in (33) will affect the steady-state value of the ratio k_p/k_f. An alternative choice to using k_p/ε_p is to use τ_p and adjust C_4 to obtain the ratio found for homogeneous CIT.

To simplify the computations, we neglect the spatial variations of the volume fraction, leading to replace the diffusive terms, in (22)–(25) and (33) with the approximation

$$\frac{1}{\langle \alpha_f \rangle} \frac{\partial}{\partial y} \left(\langle \alpha_f \rangle (\nu_{ft} + \nu_f) \frac{\partial \langle u_{f,i} u_{f,j} \rangle}{\partial y} \right) \simeq \frac{\partial}{\partial y} \left((\nu_{ft} + \nu_f) \frac{\partial \langle u_{f,i} u_{f,j} \rangle}{\partial y} \right). \tag{34}$$

As discussed in a recent work[39], neglecting spatial variations of the volume fraction is consistent with assuming that the mean fluid velocity and volume fraction reach a steady state. Otherwise, the hyperbolic form of the fluid-phase equations, along with the one-dimensional nature of the turbulence at high mass loading, results in unsteady solutions for the EE Reynolds-stress model[39].

III. CHANNEL FLOW CONFIGURATION

The present study considers a vertical channel flow of width $2W$, with the span-wise direction denoted by x, the wall-normal direction as y ($0 \leq y \leq 2W$), and the vertical stream-wise direction as z. The same flow parameters as in the reference EL-DNS[1] have been chosen and are reported in Table II. The prescribed friction Reynolds number is $Re_\tau = u_\tau W/\nu_f = 300$, where $W = 1.8$ cm is the channel half-width and u_τ is the friction velocity. The numerical discretization consists in a one-dimensional grid allocated along the wall-normal direction. Namely, a uniform grid spacing is imposed, with a total number of points $N_y = 200$, which leads to a discretization size $\Delta y^+ = 1.5$. Here, the superscript $+$ denotes normalisation with the viscous scales for length ν_f/u_τ and time ν_f/u_τ^2.

The fluid is subjected to a mean pressure gradient and to the gravity, both in the vertical

15

direction. The latter is constant, while the pressure gradient is dynamically adjusted in order to keep a constant mass flow rate after the injection of particles. Once a steady state is reached with the desired shear Reynolds number, Re_τ, particles are injected randomly with an initial velocity equal to the mean fluid velocity interpolated at the particle position. It is worth remarking that we are dealing with statistical particles, which have only the aim of reconstructing the associated statistical quantities, i.e., mean velocity, root mean square, etc. This means also that the particle volume fraction is not directly connected to the total number of particles, i.e., doubling the volume fraction does not require to double the number of particles. Indeed at the beginning of the computation the average volume fraction $\overline{\langle \alpha_p \rangle}$ is fixed, and then the local mean volume fraction $\langle \alpha_p \rangle$ is scaled to the initial one through a constant. The mean mass loading of the channel is defined by

$$\Phi = \frac{\rho_p}{\rho_f} \frac{\overline{\langle \alpha_p \rangle}}{\overline{\langle \alpha_f \rangle}}. \tag{35}$$

The mass loading ranges from $0 \leq \Phi \leq 2$ corresponding to $0 \leq \overline{\langle \alpha_p \rangle} \leq 0.001$. The density ratio is $\rho_p / \rho_f = 2000$. The particle Stokes numbers that have been considered correspond to the two sets analyzed in the EL-DNS[1], namely $St_\tau = \tau_p u_\tau / W = 0.21$ and $St_\tau = 2.1$, corresponding to a particle diameter $d_p^+ = 0.74$ and 2.35. The particle Reynolds number for these two classes of particles is $Re_p = d_p \tau_p g / \nu_f = 0.32$ and 10. The values used in the simulations are summarized in Table II. Each simulation has been performed with the same number of statistical particles $N_p = 5 \times 10^4$.

The nominal pressure gradient for the unladen case (which is known once the shear Reynolds is fixed), is dynamically adjusted in the laden cases, in order to maintain the same bulk fluid velocity in the vertical direction as in the unladen case,

$$\overline{U}_{f,z} = \frac{1}{W \overline{\langle \alpha_f \rangle}} \int_0^W \langle \alpha_f \rangle (y) \langle U_{f,z} \rangle (y) \, dy. \tag{36}$$

The same procedure was used in the time-dependent EL-DNS[1] and EE simulations[2,39].

IV.   NUMERICAL APPROACH

The fluid–particle flow is simulated through an hybrid EL algorithm. Fluid-phase equations are discretized on the uniform grid, while particle-phase equations are discretized in time through a numerical scheme suitable for SDEs, which will be described in the following. The algorithm can be decomposed in several steps:

- Evaluation of RA quantities of the particle phase (i.e., $\langle U_{p,z} \rangle$, $\langle U_{s,z} \rangle$, etc.): quantities attached to single particles are averaged over computational cells (infinite slices parallel to the wall) by means of an ensemble average and reported on the grid nodes. Calling $a^{(n)}$ a quantity attached to the nth particle, the ensemble average will be given by

$$\langle a_E \rangle = \frac{1}{N_E} \sum_{n \in \Delta_E} a^{(n)} \xrightarrow[\Delta_E \to 0]{N_E \to \infty} \langle a \rangle \tag{37}$$

where N_E is the number of particles in the cell and Δ_E is the cell size. For reliable statistics with minimal numerical dispersion, it is desirable to minimize the size of the averaging domain, namely $\Delta_E \to 0$, and maximize the number of statistical particles, namely $N_E \to \infty$, but since the Lagrangian equations are coupled with the Eulerian RA fluid-phase equations, it is not required to use finer discretization than the Eulerian grid. Indeed, that would not increase the global accuracy, but would probably lead to misleading spurious effects. Thus, for averaging Lagrangian quantities, we have used the uniform grid used to discretize the fluid-phase equations.

- Particle and fluid RA quantities that are needed in the SDEs are interpolated at each particle position with a second-order scheme.

- Equations (17) are advanced in time through a novel Euler first-order scheme for SDEs, which is inspired by the one proposed by Peirano et al.[20], but with the addition of two-way coupling terms. Namely, two-way coupling prevents from solving the three equations of $U_{s,i}$, $U_{p,i}$ and $x_{p,i}$ in cascade as typically done in dilute flows. For this reason an initial diagonalization of the system of equations is needed to uncouple the variables $U_{p,i}$ and $U_{s,i}$.

- Equations (21)–(25) and (33) are advanced in time with a finite-difference, semi-implicit scheme (viscous terms), with the addition of the two-way coupling terms with respect to classical Reynolds-stress models for single-phase flows.

- The mean pressure gradient is updated every N_{pres} steps to adjust the mass flow rate. Too rapid changes of this term may lead to numerical instabilities. Therefore, it is more suitable to reach the desired mass flow rate by steps where each time a steady state is reached before changing the pressure gradient.

Initial conditions for the fluid phase are those obtained at steady state in the dilute case (without two-way coupling).

A. Fluid phase

The Eulerian equations describing the fluid phase are discretized through a finite-difference scheme, both in space and time. For the space discretization, we have used a second-order semi-implicit centered scheme where convective non-linear terms are treated explicitly, while diffusive terms are implicit. The discretization of the mean momentum equation in the vertical direction yields:

$$\frac{\langle U_{f,z}\rangle_i^{n+1} - \langle U_{f,z}\rangle_i^n}{\Delta t} = -C_f - \frac{\langle u_{f,y}u_{f,z}\rangle_{i+1}^n - \langle u_{f,y}u_{f,z}\rangle_{i-1}^n}{2\Delta y}$$
$$+ \frac{\nu_f}{\langle \alpha_f\rangle_i^n} \frac{\langle U_{f,z}\rangle_{i+1}^{n+1} - 2\langle U_{f,z}\rangle_i^{n+1} + \langle U_{f,z}\rangle_{i-1}^{n+1}}{\Delta y^2} - g + \frac{\varphi_i^n}{\tau_p}(\langle U_{p,z}\rangle_i^n - \langle U_{s,z}\rangle_i^n) \quad (38)$$

where C_f stands for the mean pressure gradient.

For the Reynolds stresses and the fluid dissipation, we apply the same reasoning and we obtain analogous discretized equations. The six fluid variables are then grouped in a single vector

$$X = [\langle U_{f,z}\rangle \ \langle u_{f,x}u_{f,x}\rangle \ \langle u_{f,y}u_{f,y}\rangle \ \langle u_{f,z}u_{f,z}\rangle \ \langle u_{f,y}u_{f,z}\rangle \ \varepsilon_f], \quad (39)$$

of length $6N_y$, and the matrix associated to the system is built. The equations are, thus, put in the form $[A]X^{n+1} = b$, and the system is solved to find fluid quantities at $n + 1$.

No-slip boundary conditions are imposed for the mean velocity and all Reynolds stresses at the wall. At the channel center, we impose a symmetry condition with the only exception being $\langle u_{f,y}u_{f,z}\rangle$, which must be zero (anti-symmetric). The boundary condition on the fluid dissipation rate ε_f is zero flux at the wall and at the channel center.

It is worth remarking that the source terms due to two-way coupling with the particle phase are obtained by means of ensemble averages of stochastic quantities. Therefore, they can be noisy and cause numerical issues. Two strategies are used to smooth these quantities: using a high number of statistical particles (i.e., $N_p = 5 \cdot 10^4$ corresponds to an average number of particles per cell $N_{cell} = 250$), and time-averaging of the ensemble-averaged quantities.

B.   Particle phase

SDEs need an ad-hoc numerical scheme for a proper discretisation. Previously, a first-
and a second-order scheme based on analytical solutions with constant coefficients have
been proposed for the dilute regime model[20]. Yet, as a consequence of the appearance of
$\mathbf{U}_p$ in the equation of $\mathbf{U}_s$, that scheme cannot be used with the present particle model since
two-way coupling modifies the nature of the system of SDEs. This leads to a complete
coupling between the two equations of the particle and fluid velocity seen, which prevents us
from directly finding the analytical solution with constant coefficients of $\mathbf{U}_s$. The strategy
adopted in the present work has been to put the system of SDEs in diagonal form in order
to uncouple $\mathbf{U}_s$ and $\mathbf{U}_p$, as proposed for a two-way coupling model[20].

We start by considering the sub-system composed by the equations for U_p and U_s, which
can be put in vector form as follows (the i index stands for the three spatial dimensions):

$$d\mathbf{X}_i = \mathbf{C}_i \, dt + [A]_i \mathbf{X}_i \, dt + [B]_i d\mathbf{W}_i, \tag{40}$$

with

$$\mathbf{X}_i = \begin{pmatrix} U_{p,i} \\ U_{s,i} \end{pmatrix} \qquad \mathbf{C}_i = \begin{pmatrix} \langle U_{p,i} \rangle / T_{Lp} - \frac{1}{\langle \alpha_p \rangle} \frac{\partial \langle \alpha_p \rangle \langle P_{ij} \rangle}{\partial x_j} + \delta v_{p,j} \frac{\partial \langle U_{p,i} \rangle}{\partial x_j} + g_i \\ -\frac{1}{\rho_f} \frac{\partial \langle p_f \rangle}{\partial x_i} + \langle U_{f,i} \rangle / T_{L,i}^* + g_i \end{pmatrix} \tag{41}$$

$$[A]_i = \begin{bmatrix} -(1/\tau_p + 1/T_{Lp}) & 1/\tau_p \\ \varphi/\tau_p & -(1/T_{L,i}^* + \varphi/\tau_p) \end{bmatrix} \qquad [B]_i = \begin{bmatrix} C & 0 \\ 0 & B_{s,i} \end{bmatrix}. \tag{42}$$

$B_{s,i}$ is the diffusion coefficient of $U_{s,i}$, C the constant diffusion coefficient of U_p, and $d\mathbf{W}_i =
(dW_{p,i} \quad dW_{s,i})^T$. To simplify the derivation of the numerical scheme, we treat explicitly
the production term $\delta v_{p,j} \frac{\partial \langle U_{p,i} \rangle}{\partial x_j}$. Otherwise, the system would have been fully coupled, not
only in the three variables $U_p, U_s, \delta v_p$, but also in the three directional components x, y, z,
yielding a system matrix of size 9×9 to be diagonalized for each particle. With the explicit
treatment, we have to diagonalize only three 2×2 matrices.

A diagonalization of the system gives

$$d\mathbf{Y}_i = [T]_i^{-1} \mathbf{C}_i \, dt + [D]_i \mathbf{Y}_i \, dt + [T]_i^{-1} [B]_i d\mathbf{W}_i, \tag{43}$$

where $[T]_i$ and $[D]_i$ are the eigenvector matrix and the eigenvalues diagonal matrix relative to
$[A]_i$. The transformation is given by $\mathbf{X}_i = [T]_i \mathbf{Y}_i$. Now we can split for the two components

of $\mathbf{Y}_i$, and write the equations in the following form:

$$dY_{i,1} = K_{i,1}\, dt - \lambda_{i,1} Y_{i,1}\, dt + Z_{i,11}\, dW_{p,i} + Z_{i,12}\, dW_{s,i}, \tag{44}$$

$$dY_{i,2} = K_{i,2}\, dt - \lambda_{i,2} Y_{i,2}\, dt + Z_{i,21}\, dW_{p,i} + Z_{i,22}\, dW_{s,i}, \tag{45}$$

where $\lambda_{i,j}$ are the negative of the eigenvalues. Each component of the analytic solution with constant coefficients can be found looking for a solution of the form

$$Y_{i,j}(t) = H_{i,j}(t)\exp(-t\lambda_{i,j}), \tag{46}$$

with

$$dH_{i,j}(t) = \exp(t\lambda_{i,j})[K_{i,j}\, dt + Z_{i,j1}\, dW_{p,i} + Z_{i,j2}\, dW_{s,i}]. \tag{47}$$

Integration between t_0 and t gives

$$Y_{i,j}(t) = Y_{i,j}(t_0)\exp(-\Delta t\lambda_{i,j}) + \frac{K_{i,j}}{\lambda_{i,j}}[1 - \exp(-\Delta t\lambda_{i,j})]$$
$$+ Z_{i,j1}\exp(-t\lambda_{i,j})\int_{t_0}^{t}\exp(s\lambda_{i,j})dW_{p,i} + Z_{i,j2}\exp(-t\lambda_{i,j})\int_{t_0}^{t}\exp(s\lambda_{i,j})dW_{s,i}, \tag{48}$$

where $\lambda_{i,j}$, $K_{i,j}$, $Z_{i,jk}$ are frozen at time t_0. The analytical solution of $\mathbf{U}_p$ and $\mathbf{U}_s$ can be found transforming back the solution obtained, and is shown in Table I. Stochastic integrals appearing in the analytical solution can be discretized using the Cholesky algorithm. The resulting numerical scheme and the covariance matrices for the evaluation of stochastic integrals are reported in Appendix A.

The uncorrelated velocity, $\boldsymbol{\delta v}_p$, can be treated separately, considering it explicitly, since it has been uncoupled in the $\mathbf{U}_p$ equation. The production term $\delta v_{p,j}\partial\langle U_{p,i}\rangle/\partial x_j$ couples the three components of $\boldsymbol{\delta v}_p$. Thus, a diagonal decomposition would be in principle necessary to obtain three independent equations, one for each spatial component. However, as we dealt with equations (40), we have solved the equation in a explicit way (fixed at time step n), and therefore no diagonalization is needed. Recall that the stochastic process for the uncorrelated velocity is described by the following equation:

$$d\,\delta v_{p,i} = -\frac{\delta v_{p,i}}{T_\delta}\, dt + K_{\delta,ij}\, dt + B_{\delta,ij}\, dW_{\delta,j} + B_c\, dW_{c,i}, \tag{49}$$

with

$$\frac{1}{T_\delta} = \frac{1}{\tau_p} + \frac{(1+e)(3-e)}{4\tau_c}, \quad K_{\delta,ij} = \frac{1}{\langle\alpha_p\rangle}\frac{\partial\langle\alpha_p\rangle\langle P_{ij}\rangle}{\partial x_j} - \delta v_{p,j}\frac{\partial\langle U_{p,i}\rangle}{\partial x_j}, \quad B_c = \sqrt{\frac{1}{2\tau_c}(1+e)^2\langle\Theta_p\rangle}. \tag{50}$$

20

TABLE I. Analytical solutions to system (17) for time-independent coefficients. Stochastic integrals $(\gamma_{i,pj}, \gamma_{i,sj}, \sigma_{\delta,ij}, \sigma_{c,i}, \Pi_{ip}, \Pi_{is}, \Sigma_{\delta,ij}, \Sigma_{c,i})$ are shown in Table IV of Appendix A.

$$U_{p,i}(t) = \left\{ Y_{i,1}(t_0)\exp(-\Delta t\lambda_{i,1}) + \frac{K_{i,1}}{\lambda_{i,1}}[1 - \exp(-\Delta t\lambda_{i,1})] + \gamma_{i,p1} + \gamma_{i,s1} \right\}[T_{11}]_i$$

$$+ \left\{ Y_{i,2}(t_0)\exp(-\Delta t\lambda_{i,2}) + \frac{K_{i,2}}{\lambda_{i,p2}}[1 - \exp(-\Delta t\lambda_{i,2})] + \gamma_{i,p2} + \gamma_{i,s2} \right\}[T_{12}]_i\,,$$

$$U_{s,i}(t) = \left\{ Y_{i,1}(t_0)\exp(-\Delta t\lambda_{i,1}) + \frac{K_{i,1}}{\lambda_{i,1}}[1 - \exp(-\Delta t\lambda_{i,1})] + \gamma_{i,p1} + \gamma_{i,s1} \right\}[T_{21}]_i$$

$$+ \left\{ Y_{i,2}(t_0)\exp(-\Delta t\lambda_{i,2}) + \frac{K_{i,2}}{\lambda_{i,2}}[1 - \exp(-\Delta t\lambda_{i,2})] + \gamma_{i,p2} + \gamma_{i,s2} \right\}[T_{22}]_i\,,$$

$$\delta v_{p,i}(t) = \delta v_{p,i}(t_0)\exp(-\frac{\Delta t}{T_\delta}) + K_{\delta,ij} \cdot T_\delta\left[1 - \exp(-\frac{\Delta t}{T_\delta})\right] + \sigma_{\delta,ij} + \sigma_{c,i}\,,$$

$$x_{p,i}(t) = x_{p,i}(t_0) + \left\{ \frac{Y_{i,k}(t_0)}{\lambda_{i,k}}[1 - \exp(-\Delta t\lambda_{i,k})] + \frac{K_{i,k}}{\lambda_{i,k}}[\Delta t + \frac{1}{\lambda_{i,k}}(\exp(-\Delta t\lambda_{i,k}) - 1)] \right\}[T_{1k}]_i + \Pi_{ip} + \Pi_{is}$$

$$+ \delta v_{p,i}(t_0)T_\delta[1 - \exp(-\Delta t/T_\delta)] + K_{\delta,ij} \cdot T_\delta\left[\Delta t - T_\delta\left(1 - \exp(-\frac{\Delta t}{T_\delta})\right)\right]$$

$$+ \Sigma_{\delta,ij} + \Sigma_{c,i}$$

$[B_\delta]$ defined in (A1). Equation (49) is formally equal to (44). Therefore, the same derivation is adopted, leading to the following analytical solution with constant coefficients:

$$\delta v_{p,i}(t) = \delta v_{p,i}(t_0)\exp(-\Delta t/T_\delta) + K_{\delta,ij}T_\delta[1 - \exp(-\Delta t/T_\delta)]$$

$$+ B_{\delta,ij}\exp(-t/T_\delta)\int_{t_0}^t \exp(s/T_\delta)dW_{\delta,j} + B_c\exp(-t/T_\delta)\int_{t_0}^t \exp(s/T_\delta)dW_{c,i}. \quad (51)$$

Finally the equation of the particle position (1) can be solved by integrating it in time and substituting the expressions for $\mathbf{U}_p$ and $\boldsymbol{\delta v}_p$:

$$\mathbf{x}_p(t) = \mathbf{x}_p(t_0) + \int_{t_0}^t \mathbf{U}_p\, ds + \int_{t_0}^t \boldsymbol{\delta v}_p\, ds. \quad (52)$$

The complete expression is reported in Table I. Particular care must be taken in the discretization of stochastic integrals to obtain the correct correlations between variables. The detailed form of the numerical scheme is reported in Appendix A

21

V. RESULTS

A. Test of consistency with tracer particles

The numerical scheme proposed to solve the stochastic system of equations for the particle phase has been validated in the dilute case, i.e., at negligible volume fraction of the particle phase $\langle \alpha_p \rangle \to 0$. Specifically, we have tested a dilute channel with tracer particles of vanishing inertia, i.e., $\tau_p \to 0$. We have compared our results with the ones obtained for the dilute model of Peirano *et al.*[20]. From the results, it is evident that the model for dense flows recovers the dilute model solution, and that both are consistent with the average fluid solution. Indeed, from the particle equations, it can be shown that for $\tau_p \to 0$, $U_p \to U_s$ instantaneously, and that at an average level $\langle U_s \rangle \to \langle U_f \rangle$, and the same for higher-order statistics.

For this test case, the shear Reynolds number is $Re_\tau = 300$, and the particle timescale is $\tau_p = 10^{-6}$. All other parameters are the same as for the inertial particles test cases, and are reported in Table II. For both models, we have used the same values of the constants obtained from the CIT homogeneous study[38]. Their values are reported in Table III. A side-by-side comparison is made in Figure 1 between the numerical scheme for one-way coupling[20] (left panels) and the numerical scheme for two-way coupling (right panels), at $\varphi = 0$. From top to bottom are reported the mean velocity and the three diagonal components of the Reynolds stresses. Statistics related to particles are obtained averaging locally inside the cell and in time over a window of $N_{steps} = 10^5$, so of duration $\Delta t = N_{steps} \times dt = 10\ s$. It can be seen that the two numerical schemes are fully consistent, and that their solutions tend to the RA result. Indeed U_s and U_p are exactly superimposed and empty symbols corresponding to U_s are barely visible.

B. Inertial particles with two-way coupling

Some of the EL-DNS cases[1] have been reproduced, namely particles with small and large Stokes number $St = 0.21, 2.1$ with different mass loading, starting from zero up to $\varphi = 2$. To reach the higher values of the volume fraction, we have continuously increased it starting from zero in order to avoid numerical instabilities. At each intermediate steps, we had to wait for the simulation to reach a stationary state. We start by showing results at mass

Physical parameters

u_τ	shear velocity	$0.3\ m\ s^{-1}$
$U_{b(DNS)}$	bulk velocity	$5.02\ m\ s^{-1}$
$U_{b(RANS)}$	bulk velocity	$3.35\ m\ s^{-1}$
δ	channel half width	$1.8\ cm$
$\frac{dp_f}{dz}$	pressure gradient	$14.81\ Pa$
g	gravity acceleration	$-9.81\ m\ s^{-2}$
ρ_p	particle density	$2000\ kg\ m^{-3}$
ρ_f	fluid density	$1\ kg\ m^{-3}$
ν_f	fluid kinematic viscosity	$1.8 \times 10^{-5}\ m^2\ s^{-1}$
τ_p	particle relaxation time 10^{-6} ; $\quad$ 0.0128 ; $\quad$ 0.128 s	
dt	time step	$10^{-4}\ s$

TABLE II. Fluid and particle parameters used in the simulations, in accordance with the EL-DNS cases[1]. The corresponding shear Reynolds number is $Re_\tau = 300$.

C_{0f}	C_{0p}	$C_{\varepsilon 1}$	$C_{\varepsilon 2}$	C_{3f}	C_{3p}	C_4	f_s	β	C_{2f}
3.5	0.18	1.44	1.92	3.5	7.0	6.81	0.4	1	0

TABLE III. Model constants.

loading zero $\varphi = 0$ compared to the EL-DNS in order to show the initial bias between the two solutions. Indeed, it is worth remembering that we are using a relatively simple Reynolds-stress model (Rotta, since C_{2f} has been set to zero) to describe the fluid phase and that a perfect recovery of the DNS solution cannot be expected in this case[33,39]. To obtain a better agreement, more complex models can be used such as, for instance, the non-local elliptic relaxation model[46]. The use of such models is out of the scope of this work, as we are mainly focused on showing the relative trend with respect to mass loading. Figure 2 shows fluid-phase statistics from RANS and EL-DNS for the average vertical velocity and Reynolds stresses.
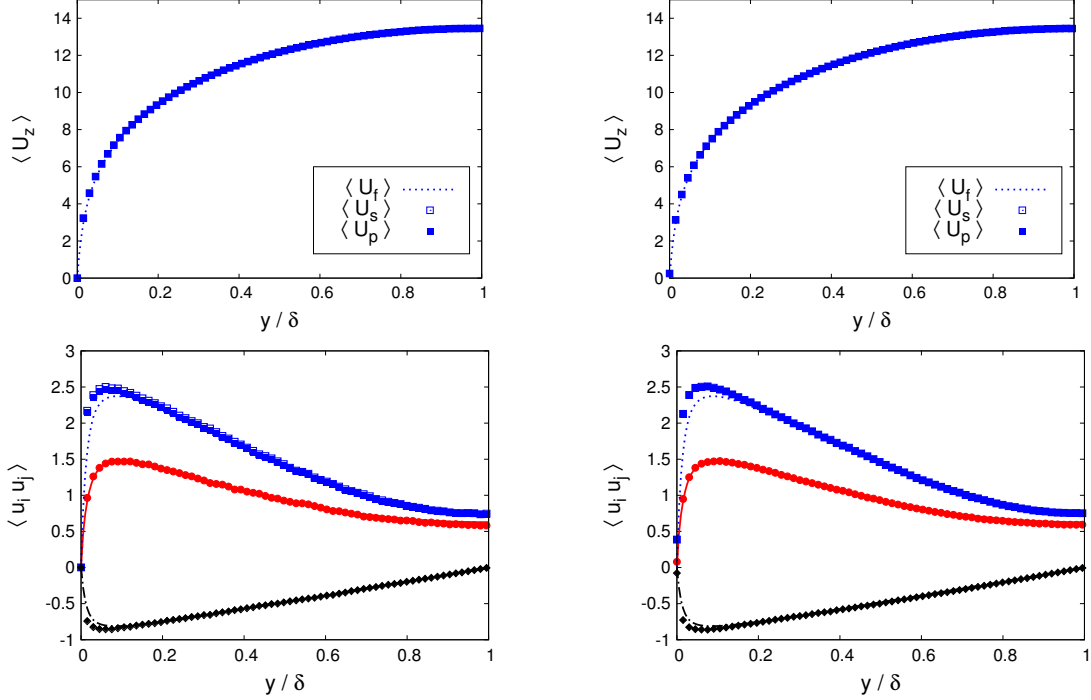
FIG. 1. Mean velocity and Reynolds stresses with tracer particles ($\tau_p = 10^{-6}$) in the dilute limit ($\varphi = 0$). Left panels are results with the numerical scheme for one-way coupling[20], and right panels are results with the new numerical scheme. All quantities are made dimensionless with the shear velocity $u_\tau = 0.3\,m/s$. RA fluid velocity (lines), fluid velocity seen by particles (symbols), particle velocity (filled symbols). $\langle u_{f,y}u_{f,y}\rangle$ (red solid line), $\langle u_{f,z}u_{f,z}\rangle$ (blue dotted line), $\langle u_{f,y}u_{f,z}\rangle$ (black dash dotted line), $\langle u_{s,y}u_{s,y}\rangle$ (red empty circles), $\langle u_{s,z}u_{s,z}\rangle$ (blue empty squares), $\langle u_{s,y}u_{s,z}\rangle$ (black empty diamonds), $\langle u_{p,y}u_{p,y}\rangle$ (red filled circles), $\langle u_{p,z}u_{p,z}\rangle$ (blue filled squares), $\langle u_{p,y}u_{p,z}\rangle$ (black filled diamonds) .

1.   *Mean velocities*

We analyze here the mean velocities of the fluid–particle flow. In Figures 3 and 4, we compare the average velocities of the fluid and of particles from the model to the respective ones of the EL-DNS[1], at different mass loading. In these figures, velocities are made non-dimensional with the EL-DNS, and the model bulk velocity, i.e., $U_b = 5.02m/s$ for the DNS, and $U_b = 3.345m/s$ for the model. It is evident that the model is able to capture the modulation that the particles exert on the fluid when varying the volume fraction of the particle phase for both Stokes numbers. Moreover, the model seems to be too sensitive to
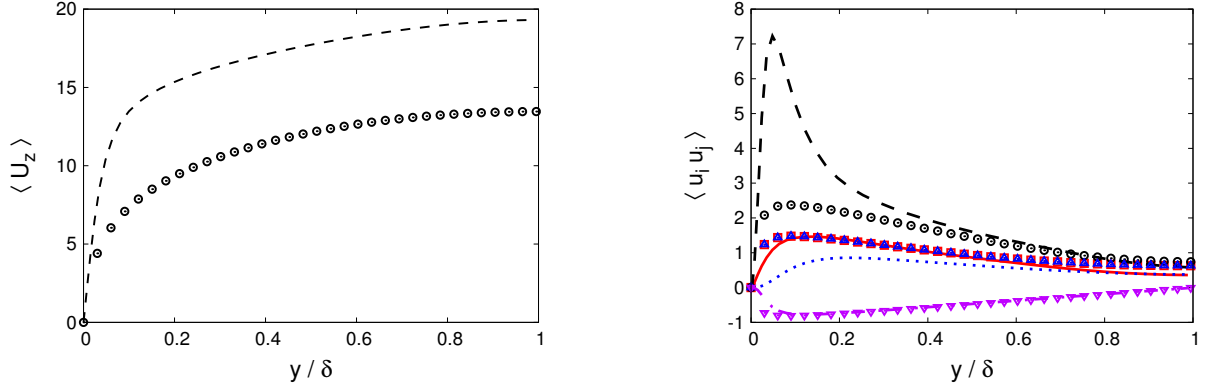
24

FIG. 2. Mean velocity and Reynolds stresses of the fluid phase at $\varphi = 0$. Lines corresponds to EL-DNS[1], symbols to the model. Velocities and Reynolds-stresses have been made non-dimensional with u_τ. $\langle u_{f,x} u_{f,x} \rangle$ (red solid line, squares), $\langle u_{f,y} u_{f,y} \rangle$ (blue dotted line, triangles), $\langle u_{f,z} u_{f,z} \rangle$ (black dashed line, circles), $\langle u_{f,y} u_{f,z} \rangle$ (magenta dash dotted line, downward triangles).
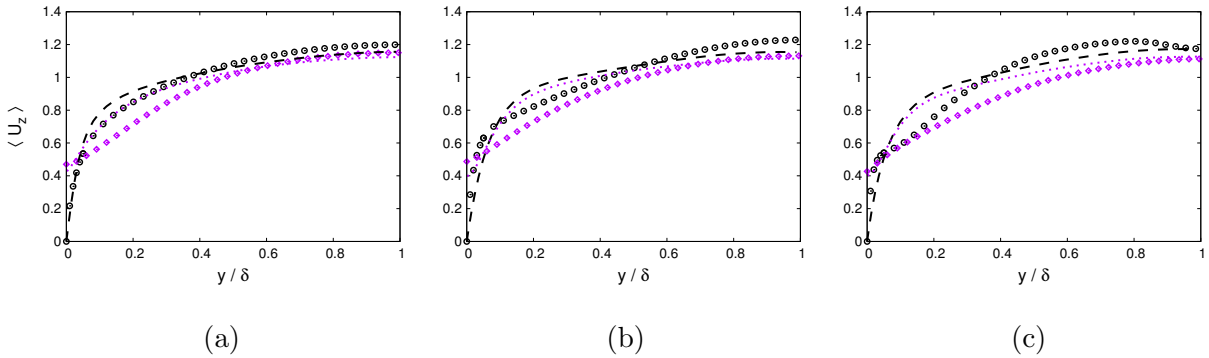

(a)   (b)   (c)

FIG. 3. Mean velocity of the fluid and particle phases at different mass loading for $St = 0.21$ particles. Lines corresponds to EL-DNS[1], symbols to the model. Velocities are divided by the corresponding fluid bulk velocity, $U_{b(DNS)}$ and $U_{b(RANS)}$. $\langle U_{f,z} \rangle$ (black dashed line, circles), $\langle U_{p,z} \rangle$ (magenta dotted line, diamonds). $\varphi = 0.2$ (a), $\varphi = 1$ (b), $\varphi = 2$ (c)

mass loading, and yet the particle-phase velocity exhibits a significant slip at the wall, as expected, and its prediction is good near the wall and at the channel center.

It is known that the drift velocity is sensitive to the model constants[39,43], and in particular to C_2, which in the present case has been set to zero. Specifically, constants have been tuned for a homogeneous CIT case at $\varphi = 20$. Therefore, it is not surprising that at low-mass-loading the results are not fully satisfactory. If we look at the relative variations with respect
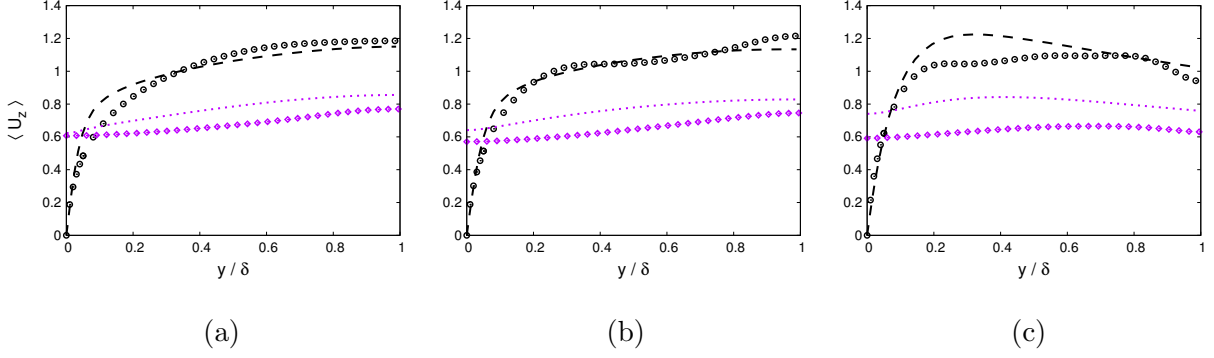
25

FIG. 4. Mean velocity of the fluid and particle phases at different mass loading for $St = 2.1$ particles. Lines corresponds to EL-DNS[1], symbols to the model. Velocities are divided by the corresponding fluid bulk velocity, $U_{b(DNS)}$ and $U_{b(RANS)}$. $\langle U_{f,z} \rangle$ (black dashed line, circles), $\langle U_{p,z} \rangle$ (magenta dotted line, diamonds). $\varphi = 0.2$ (a), $\varphi = 1$ (b), $\varphi = 2$ (c)
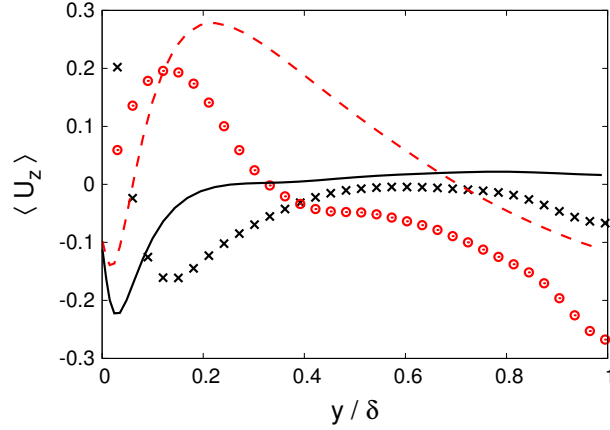

FIG. 5. Variations of the mean fluid velocity at $\varphi = 2$ with respect to the solution at $\varphi = 0$. Lines corresponds to EL-DNS[1], symbols to the model. $St = 0.21$ (solid black line, $\times$), $St = 2.1$ (dashed red line, $\circ$).

to the reference value at $\varphi = 0$:

$$\mathcal{Q}_r = \frac{\mathcal{Q}(\varphi) - \mathcal{Q}(\varphi = 0)}{\mathcal{Q}(\varphi = 0)} , \tag{53}$$

see Figure 5, the trend with mass loading bodes well for further tests at higher values.

2. Energy

The kinetic energies for the fluid and particle phases are compared in Figures 6 and 7. As discussed earlier for the mean velocity, a quantitative agreement is not expected, and a
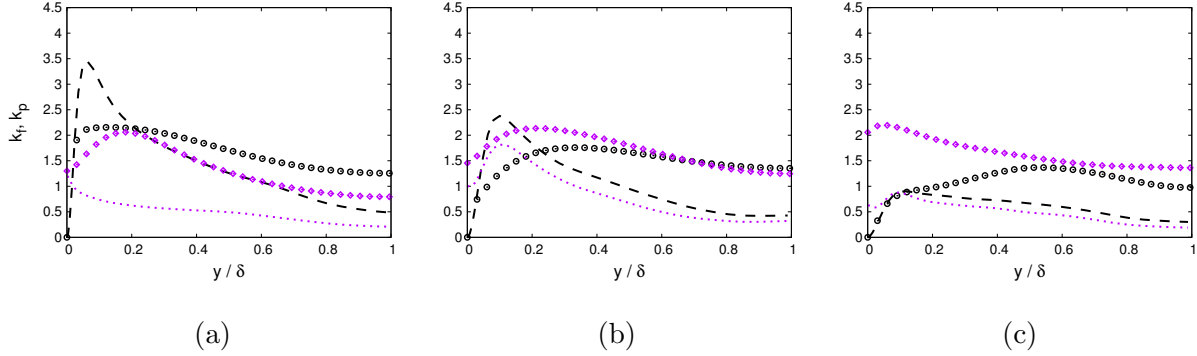
26

FIG. 6. Energy of the fluid and particle phases at different mass loading for $St = 0.21$. Lines corresponds to EL-DNS[1], symbols to the model. Energy is divided by u_τ^2. k_f (black dashed line, circles), k_p (magenta dotted line, diamonds). $\varphi = 0.2$ (a), $\varphi = 1$ (b), $\varphi = 2$ (c)

better optimization of the constants would be needed. Nevertheless, it is interesting how the model is able to capture the decrease of the fluid kinetic energy when increasing the volume fraction, for both Stokes number. It has been shown[1] that there is a flow transition at mass loading around $\varphi = 2$, and that above this value the energy increases again. The reason is that after a laminarization of the flow due to the presence of particles, clusters start to become dominant, and their fluctuations induce CIT-like turbulence again in the fluid phase. Therefore it is encouraging that even if the constants have been optimized for CIT, the model behaves well qualitatively also at low volume fraction where the mechanism of energy transfer is qualitatively different.

Concerning the particle-phase energy, for $St = 0.21$ we see that after an initial increase from $\varphi = 0.2$ to $\varphi = 1$, the model describes consistently the EL-DNS results. At $\varphi = 2$, we have a further increase instead of a reduction. Nevertheless, the fact that the $k_p > k_f$ is inconsistent, and was not observed in the EE Reynolds-stress model[39]. This mismatch is most likely due to the values assigned to the model constants that have been optimized in the homogeneous CIT for a higher Stokes number. Indeed, for the case at $St = 2.1$, the qualitative trend is much closer to the EL-DNS results for both fluid and particle kinetic energies.

In Figure 8, we show the trend of the average fluid turbulent kinetic energy with respect to the mass loading. As outlined above, the model predicts well the energy decrease, and apart from an initial bias, which is present only for the small Stokes number, the relative variations are in very good agreement with the EL-DNS results.
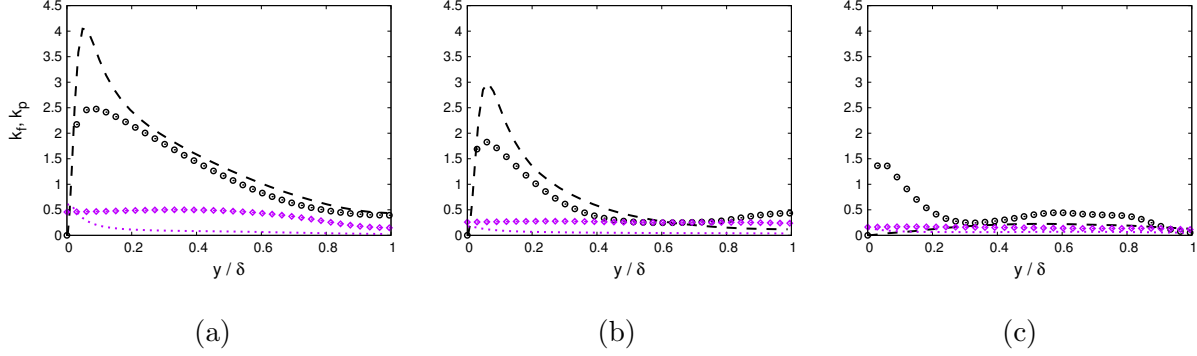
FIG. 7. Energy of the fluid and particle phases at different mass loading for $St = 2.1$. Lines corresponds to EL-DNS[1], symbols to the model. Energy is divided by u_τ^2. k_f (black dashed line, circles), k_p (magenta dotted line, diamonds). $\varphi = 0.2$ (a), $\varphi = 1$ (b), $\varphi = 2$ (c)
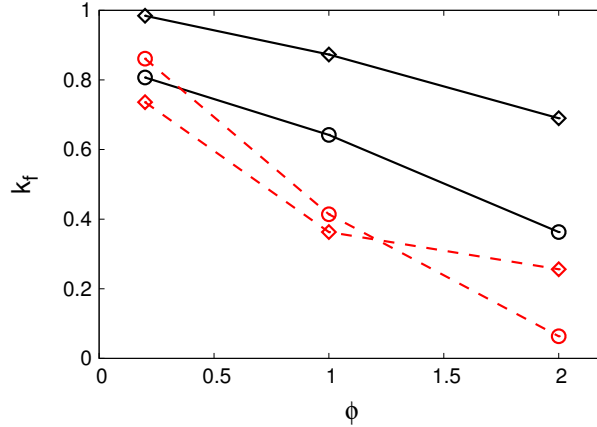

FIG. 8. Fluid-phase energy variations with respect to the mass loading normalized by the corresponding energy at $\varphi = 0$. EL-DNS data[1] ($\circ$), model ($\diamond$). $St = 0.21$ (solid black lines), $St = 2.1$ (dashed red lines).

Finally, we report the anisotropy of the Reynolds stresses in Figures 9 and 10. In homogeneous CIT, the Reynolds stresses are highly anisotropic with the zz component significantly larger than the other two, and the yz component is zero. In the channel case, we note that the anisotropy becomes more and more pronounced when increasing the mass loading and thus moving towards CIT. The agreement with the EL-DNS results is satisfactory and the zz contribution to k_f increase from an initial 50% to above 80% for $\varphi = 2$ in the inner part of the channel.

As expected, the fluid-phase turbulence approaches the one-dimensional limit as the mass fraction increases due to the drag-production term. The same behavior was observed with
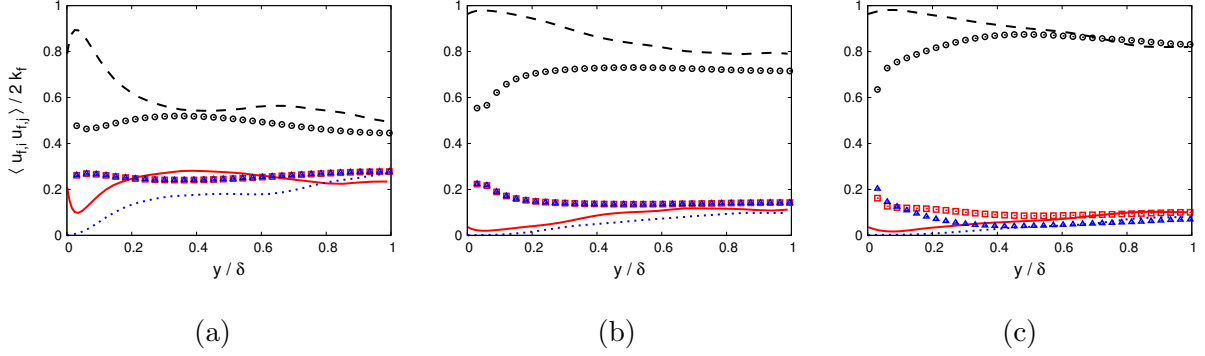
28

FIG. 9. Fluid-phase Reynolds-stress components at different mass loading at $St = 0.21$. Lines corresponds to EL-DNS[1], symbols to the model. $\langle u_{f,x} u_{f,x} \rangle$ (red solid line, squares), $\langle u_{f,y} u_{f,y} \rangle$ (blue dotted line, triangles), $\langle u_{f,z} u_{f,z} \rangle$ (black dashed line, circles). $\varphi = 0.2$ (a), $\varphi = 1$ (b), $\varphi = 2$ (c)

FIG. 10. Fluid-phase Reynolds-stress components at different mass loading at $St = 2.1$. Lines corresponds to EL-DNS[1], symbols to the model. $\langle u_{f,x} u_{f,x} \rangle$ (red solid line, squares), $\langle u_{f,y} u_{f,y} \rangle$ (blue dotted line, triangles), $\langle u_{f,z} u_{f,z} \rangle$ (black dashed line, circles). $\varphi = 0.2$ (a), $\varphi = 1$ (b), $\varphi = 2$ (c)
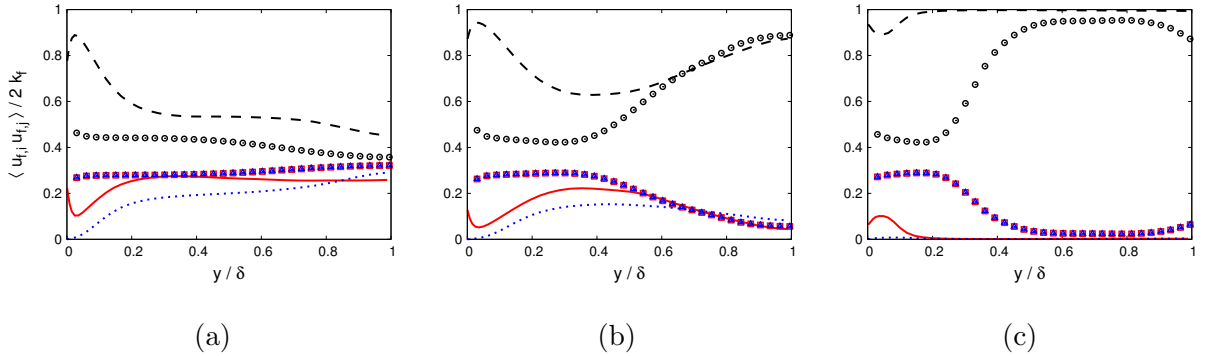
the EE Reynolds-stress model[39]. However, the present EL model reproduces correctly this mechanism only in the inner part of the channel, while approaching the wall the Reynolds stresses remain more isotropic than in the EL-DNS. This discrepancy is probably due to the original bias of the RA fluid model, which is evident at $\varphi = 0$ in Figure 2.

VI. CONCLUSIONS

In this work, we report on the application of the stochastic model for dense particle-laden flows proposed for homogeneous CIT[38] to turbulent channel flows. We have rewritten

the model equations for inhomogeneous applications, and then proposed a new numerical scheme for the solution of these SDEs. In particular, the particle-phase equations have been solved numerically using a Monte–Carlo approach.

It is worth stressing that these SDEs present new numerical difficulties due to two-way coupling with respect to already existing models for dilute flows[20]. The particle and the fluid-seen velocity equations are fully coupled and, therefore, an initial diagonalization of the system is needed for each statistical particle. Then, a numerical scheme is derived based on the analytical solution that the equations admit with constant coefficients. The scheme includes the additional terms that are present in the particle velocity equations with respect to the dilute model, as well as the new equations for the uncorrelated component of the particle velocity δv_p.

A turbulent channel flow at shear Reynolds number $Re_\tau = 300$ has been simulated, reproducing the same configuration as in a recent EL-DNS[1]. The numerical scheme has been validated in a test of consistency with tracer particles at negligible mass loading, and the solution has been compared to that obtained with the numerical scheme for dilute flows for the same flow conditions. Direct comparison shows that the scheme reproduces exactly the same results as those with the dilute scheme, and that in both cases an excellent consistency is obtained, i.e., the solution from the Lagrangian tracer particles recovers the one from the Eulerian fluid-phase RA equations.

Inertial particles with Stokes number $St = 0.21$ and 2.1 have been simulated at different mass loading, reproducing some of the EL-DNS cases. Since the purpose of the present work is to assess the capability of the Lagrangian stochastic model to adapt to inhomogeneous cases, the values of the model constants have not been changed from those obtained in the homogeneous CIT case[38], which was for high-Stokes-number particles at a mass loading of $\varphi = 20$. Thus, the agreement with EL-DNS is expected to be only qualitative, since we have tested only cases at mass loading $0 \leq \varphi \leq 2$. The importance of developing a Lagrangian stochastic approach resides in the fact that some quantities are available in a closed form, most notably $\mathbf{U}_s$, which are difficult to approximate in the EE RANS approach. The present work is the first step in this direction.

Results have shown that the model is able to capture some modulation due to the particles on the fluid velocity, even though the variations of the mean velocity profile appear to be too sensitive to the mass loading for the small Stokes number. However, the constant

reduction of turbulent kinetic energy is well captured, and the re-partition of energy between the different Reynolds-stress components is in decent agreement with EL-DNS. It is worth remarking that the strong anisotropy of the Reynolds-stress tensor in CIT is one of its key features. Therefore, the trend obtained up to $\varphi = 2$ is positive and bodes well for higher mass loading.

Overall, the results are very encouraging. In fact, even with constants optimized for CIT, the model exhibits good trends with respect to the mass loading. It has been discussed[1] how different regimes are encountered when increasing the volume fraction, from weak interphase coupling ($\varphi \leq 1$) where the dominant mechanism for generating fluid-phase turbulent kinetic energy is the mean-shear production, to moderate coupling ($2 \leq \varphi \leq 4$) where the flow relaminarizes, to strong coupling ($\varphi \geq 10$) with CIT. Therefore, since different mechanisms are at play, we can not expect to obtain a quantitative agreement for all cases by keeping the same values for the constants. Moreover, as shown in a recent work[39], the one-dimensional nature of CIT leads to time-dependent solutions for a EE Reynolds-stress model, which is likely to also be the case with the Lagrangian model discussed in the work.

Some words are in order on how to improve the predictions of the model. The discrepancy in the near-wall region, notably in terms of anisotropy, could be improved by adopting a more refined RANS fluid model. As we have shown in the uncoupled case ($\varphi = 0$), the fluid model used in this work lacks for a proper description of the mean fluid velocity and Reynolds stresses, especially in the boundary layer. This background error is of course present also at higher mass loading, and therefore a quantitative improvement of the results can only be obtained starting with a more refined fluid model accounting for a specific treatment of the near-wall region[33]. However, since the fluid and particle descriptions are coupled, changing the fluid model would imply different closures for the particle model, with different model constants[47]. We have decided to stick to a version of the model that has already been validated, at least in a homogeneous case, in order to have a better control of the behavior of the model and to understand whether the deficiencies are to be implied to the fluid, to the particle model, or to an improper optimization of the constants. Future works with different RANS models would help clarify this point.

Then, an exhaustive parametric study used to caliber the model will be needed before considering new applications. In this analysis, a comparison between the different versions of the model could be interesting in future work to understand at what point the additional

physics included in the complete model, notably collisions, starts to be crucial.

As future perspective, it would be of great interest to test the model also at higher mass loading in the CIT range. Because of the low computational cost of the steady-state simulations, we can adopt techniques of uncertainty quantification to find a suitable set of constants capable of reproducing all cases with acceptable accuracy in order to make the model viable for practical applications.

Data availability

The data that support the findings of this study are available from the corresponding author upon reasonable request.

Appendix A: Modeling and numerical complements

In this appendix, we briefly report some modeling complements omitted in the main text and additional details on the numerical scheme that has been developed.

The diffusion matrix $B_{\delta,ij}$ present in Equation (5) has been obtained using a Choleski decomposition[38], and reads as follows:

$$
\begin{aligned}
B_{\delta,11} &= \left[f_s \frac{\varepsilon_p}{k_p} \langle u_{p,1} u_{p,1} \rangle + (1 - f_s) \frac{2}{3} \varepsilon_p \right]^{1/2}, \\
B_{\delta,i1} &= \frac{1}{B_{\delta,11}} f_s \frac{\varepsilon_p}{k_p} \langle u_{p,i} u_{p,1} \rangle, \quad 1 < i \leq 3 \\
B_{\delta,ii} &= \left[f_s \frac{\varepsilon_p}{k_p} \langle u_{p,i} u_{p,i} \rangle + (1 - f_s) \frac{2}{3} \varepsilon_p - \sum_{j=1}^{i-1} B_{\delta,ij}^2 \right]^{1/2}, \quad 1 < i \leq 3 \quad\quad (A1) \\
B_{\delta,ij} &= \frac{1}{B_{\delta,jj}} \left(f_s \frac{\varepsilon_p}{k_p} \langle u_{p,i} u_{p,j} \rangle - \sum_{k=1}^{j-1} B_{\delta,ik} B_{\delta,jk} \right), \quad 1 < j < i \leq 3 \\
B_{\delta,ij} &= 0, \quad i < j \leq 3 \, ;
\end{aligned}
$$

The analytical solution with constant coefficients shown in Table I has a few terms that have been left in implicit form involving time integrals of stochastic processes. Their complete expressions are shown in Table IV.

The following Table V is the discrete version of Tables I and IV. It is worth noting that the analytical stochastic integrals are simulated with a proper combination of independent

32

TABLE IV. Analytical expressions of the stochastic integrals appearing in Table I.

$$\gamma_{i,p1}(t) = Z_{i,11}\exp(-t\lambda_{i,1})\int_{t_0}^{t}\exp(s\lambda_{i,1})dW_{p,i}, \quad \gamma_{i,s1}(t) = Z_{i,12}\exp(-t\lambda_{i,1})\int_{t_0}^{t}\exp(s\lambda_{i,1})dW_{s,i},$$

$$\gamma_{i,p2}(t) = Z_{i,21}\exp(-t\lambda_{i,2})\int_{t_0}^{t}\exp(s\lambda_{i,2})dW_{p,i}, \quad \gamma_{i,s2}(t) = Z_{i,22}\exp(-t\lambda_{i,2})\int_{t_0}^{t}\exp(s\lambda_{i,2})dW_{s,i},$$

$$\Gamma_{i,p1}(t) = \int_{t_0}^{t}\gamma_{i,p1}(s)\,ds, \quad \Gamma_{i,s1}(t) = \int_{t_0}^{t}\gamma_{i,s1}(s)\,ds,$$

$$\Gamma_{i,p2}(t) = \int_{t_0}^{t}\gamma_{i,p2}(s)\,ds, \quad \Gamma_{i,s2}(t) = \int_{t_0}^{t}\gamma_{i,s2}(s)\,ds,$$

$$\Pi_{ip}(t) = \Gamma_{i,p1}(t)[T_{11}]_i + \Gamma_{i,p2}(t)[T_{12}]_i, \quad \Pi_{is}(t) = \Gamma_{i,s1}(t)[T_{11}]_i + \Gamma_{i,s2}(t)[T_{12}]_i,$$

$$\sigma_{\delta,ij}(t) = B_{\delta,ij}\exp(-t/T_\delta)\int_{t_0}^{t}\exp(s/T_\delta)dW_{\delta,i},$$

$$\sigma_{c,i}(t) = B_c\exp(-t/T_\delta)\int_{t_0}^{t}\exp(s/T_\delta)dW_{c,i},$$

$$\Sigma_{\delta,ij}(t) = \int_{t_0}^{t}\sigma_{\delta,ij}(s)\,ds, \quad \Sigma_{c,i}(t) = \int_{t_0}^{t}\sigma_{c,i}(s)\,ds.$$

Gaussian random variables obtained from a Choleski decomposition. The coefficients of such expressions are obtained from the covariance matrix shown in Table VI.

TABLE V. First-order temporal discretization (Euler scheme)

Numerical integration of the system:

$$U_{p,i}^{n+1} = \left\{Y_{i,1}^n \exp(-\Delta t\lambda_{i,1}^n) + \frac{K_{i,1}^n}{\lambda_{i,1}^n}[1 - \exp(-\Delta t\lambda_{i,1}^n)] + \gamma_{i,p1}^n + \gamma_{i,s1}^n\right\}[T_{11}]_i$$

$$+ \left\{Y_{i,2}^n \exp(-\Delta t\lambda_{i,2}^n) + \frac{K_{i,2}^n}{\lambda_{i,2}^n}[1 - \exp(-\Delta t\lambda_{i,2}^n)] + \gamma_{i,p2}^n + \gamma_{i,s2}^n\right\}[T_{12}]_i^n ,$$

$$U_{s,i}^{n+1} = \left\{Y_{i,1}^n \exp(-\Delta t\lambda_{i,1}^n) + \frac{K_{i,1}^n}{\lambda_{i,1}^n}[1 - \exp(-\Delta t\lambda_{i,1}^n)] + \gamma_{i,p1}^n + \gamma_{i,s1}^n\right\}[T_{21}]_i^n$$

$$+ \left\{Y_{i,2}^n \exp(-\Delta t\lambda_{i,2}^n) + \frac{K_{i,2}^n}{\lambda_{i,2}^n}[1 - \exp(-\Delta t\lambda_{i,2}^n)] + \gamma_{i,p2}^n + \gamma_{i,s2}^n\right\}[T_{22}]_i^n ,$$

$$\delta v_{p,i}^{n+1} = \delta v_{p,i}^n \exp(-\frac{\Delta t}{T_\delta^n}) + K_{\delta,ij}^n \cdot T_\delta^n\left[1 - \exp(-\frac{\Delta t}{T_\delta^n})\right] + \sigma_{\delta,ij}^n + \sigma_{c,i}^n ,$$

$$x_{p,i}^{n+1} = x_{p,i}^n + \left\{\frac{Y_{i,k}^n}{\lambda_{i,k}^n}[1 - \exp(-\Delta t\lambda_{i,k}^n)] + \frac{K_{i,k}^n}{\lambda_{i,k}^n}[\Delta t + \frac{1}{\lambda_{i,k}^n}(\exp(-\Delta t\lambda_{i,k}^n) - 1)]\right\}[T_{1k}]_i^n + \Pi_{ip}^n + \Pi_{is}^n$$

$$+ \delta v_{p,i}^n T_\delta^n[1 - \exp(-\Delta t/T_\delta^n)] + K_{\delta,ij}^n \cdot T_\delta^n\left[\Delta t - T_\delta^n\left(1 - \exp(-\frac{\Delta t}{T_\delta^n})\right)\right]$$

$$+ \Sigma_{\delta,ij}^n + \Sigma_{c,i}^n,$$

The stochastic integrals are simulated by (analogously for $\sigma_{\delta,ij}^n$ and $\sigma_{c,i}^n$):

$$\gamma_{i,p1}^n = P_{11p}^i\, \mathcal{G}_{1,i}, \qquad\qquad\qquad \gamma_{i,s1}^n = P_{11s}^i\, \mathcal{G}_{4,i}$$

$$\gamma_{i,p2}^n = P_{21p}^i\, \mathcal{G}_{1,i} + P_{22p}^i\, \mathcal{G}_{2,i}, \qquad\qquad \gamma_{i,s2}^n = P_{21s}^i\, \mathcal{G}_{4,i} + P_{22s}^i\, \mathcal{G}_{5,i}$$

$$\Pi_{ip}^n = P_{31p}^i\, \mathcal{G}_{1,i} + P_{32p}^i\, \mathcal{G}_{2,i} + P_{33p}^i\, \mathcal{G}_{3,i}, \qquad \Pi_{is}^n = P_{31s}^i\, \mathcal{G}_{4,i} + P_{32s}^i\, \mathcal{G}_{5,i} + P_{33s}^i\, \mathcal{G}_{6,i}$$

where $\mathcal{G}_{k,i}$ are independent $\mathcal{N}(0,1)$ random variables.

The coefficients $P_{11p}^i,\ P_{21p}^i,\ P_{22p}^i,\ P_{31p}^i,\ P_{32p}^i,\ P_{33p}^i,$ (analogously for P_{ijs}) are defined as

$$P_{11p}^i = \sqrt{\langle(\gamma_{i,p1}^n)^2\rangle},$$

$$P_{21p}^i = \frac{\langle\gamma_{i,p1}^n\gamma_{i,p2}^n\rangle}{\sqrt{\langle(\gamma_{i,p1}^n)^2\rangle}}, \quad P_{22p}^i = \sqrt{\langle(\gamma_{i,p2}^n)^2\rangle - \frac{\langle\gamma_{i,1}^n\gamma_{i,p2}^n\rangle^2}{\langle(\gamma_{i,p1}^n)^2\rangle}},$$

$$P_{31p}^i = \frac{\langle\gamma_{i,p1}^n\Pi_{ip}^n\rangle}{\sqrt{\langle(\gamma_{i,p1}^n)^2\rangle}}, \quad P_{32p}^i = \frac{1}{P_{22p}^i}(\langle\gamma_{i,p2}^n\Pi_i^n\rangle - P_{21p}^iP_{31p}^i), \quad P_{33p}^i = \sqrt{\langle(\Pi_{ip}^n)^2\rangle - P_{31p}^{i2} - P_{32p}^{i2}}.$$

TABLE VI. Covariance matrix

$$\langle \gamma_{i,p1}^2 \rangle = \frac{1}{2} \frac{Z_{i,11}^2}{\lambda_{i,1}} \Big(1 - \exp(-2\Delta t \lambda_{i,1}) \Big)$$

$$\langle \gamma_{i,p2}^2 \rangle = \frac{1}{2} \frac{Z_{i,21}^2}{\lambda_{i,2}} \Big(1 - \exp(-2\Delta t \lambda_{i,2}) \Big)$$

$$\langle \gamma_{i,p1}\gamma_{i,p2} \rangle = \frac{1}{2} \frac{Z_{i,11} Z_{i,21}}{(\lambda_{i,1} + \lambda_{i,2})} \Big(1 - \exp(-\Delta t(\lambda_{i,1} + \lambda_{i,2})) \Big)$$

$$\langle \gamma_{i,p1}\Pi_{ip} \rangle = -\frac{T[1,1]_i}{2\lambda_{i,1}^2} Z_{i,11}^2 \Big(1 - \exp(-2\Delta t \lambda_{i,1}) \Big) - \frac{T[1,2]_i}{\lambda_{i,2}(\lambda_{i,1} + \lambda_{i,2})} Z_{i,11} Z_{i,21} \Big(1 - \exp(-\Delta t(\lambda_{i,1} + \lambda_{i,2})) \Big)$$

$$+ \frac{Z_{i,11}}{\lambda_{i,1}} \Big(T[1,1]_i \frac{Z_{i,11}}{\lambda_{i,1}} + T[1,2]_i \frac{Z_{i,21}}{\lambda_{i,2}} \Big) \Big(1 - \exp(-\Delta t \lambda_{i,1}) \Big)$$

$$\langle \gamma_{i,p2}\Pi_{ip} \rangle = -\frac{T[1,2]_i}{2\lambda_{i,2}^2} Z_{i,21}^2 \Big(1 - \exp(-2\Delta t \lambda_{i,2}) \Big) - \frac{T[1,1]_i}{\lambda_{i,1}(\lambda_{i,1} + \lambda_{i,2})} Z_{i,11} Z_{i,21} \Big(1 - \exp(-\Delta t(\lambda_{i,1} + \lambda_{i,2})) \Big)$$

$$+ \frac{Z_{i,21}}{\lambda_{i,2}} \Big(T[1,1]_i \frac{Z_{i,11}}{\lambda_{i,1}} + T[1,2]_i \frac{Z_{i,21}}{\lambda_{i,2}} \Big) \Big(1 - \exp(-\Delta t \lambda_{i,2}) \Big)$$

$$\langle \Pi_{ip}^2 \rangle = -\frac{T[1,1]_i^2}{2\lambda_{i,1}^3} Z_{i,11}^2 \Big(1 - \exp(-2\Delta t \lambda_{i,1}) \Big) + \frac{T[1,2]_i^2}{2\lambda_{i,2}^3} Z_{i,21}^2 \Big(1 - \exp(-2\Delta t \lambda_{i,2}) \Big) +$$

$$\Big(\frac{T[1,1]_i Z_{i,11}}{\lambda_{i,1}} + \frac{T[1,2] Z_{i,21}}{\lambda_{i,2}} \Big)^2 \Delta t + 2 \frac{T[1,1]_i T[1,2]_i}{\lambda_{i,1} \lambda_{i,2}(\lambda_{i,1} + \lambda_{i,2})} Z_{i,11} Z_{i,21} \Big(1 - \exp(-\Delta t(\lambda_{i,1} + \lambda_{i,2})) \Big)$$

$$- 2T[1,1]_i \frac{Z_{i,11}}{\lambda_{i,1}^2} \Big(T[1,1]_i \frac{Z_{i,11}}{\lambda_{i,1}} + T[1,2]_i \frac{Z_{i,21}}{\lambda_{i,2}} \Big) \Big(1 - \exp(-\Delta t \lambda_{i,1}) \Big)$$

$$- 2T[1,2]_i \frac{Z_{i,21}}{\lambda_{i,2}^2} \Big(T[1,1]_i \frac{Z_{i,11}}{\lambda_{i,1}} + T[1,2]_i \frac{Z_{i,21}}{\lambda_{i,2}} \Big) \Big(1 - \exp(-\Delta t \lambda_{i,2}) \Big)$$

REFERENCES

[1] J. Capecelatro, O. Desjardins, and R. O. Fox. On the transition between turbulence regimes in particle-laden channel flows. *J. Fluid. Mech.*, 845:499–519, 2018.

[2] M. C. Baker, B. Kong, J. Capecelatro, O. Desjardins, and R. O. Fox. Direct comparison of Eulerian–Eulerian and Eulerian–Lagrangian simulations for particle-laden vertical channel flow. *AIChE J.*, 66(7):e16230, 2020.

[3] L. P. Wang and M. R. Maxey. Settling velocity and concentration distribution of heavy particles in homogeneous isotropic turbulence. *J. Fluid. Mech.*, 256(1):27–68, 1993.

[4] J. K. Eaton and J. R. Fessler. Preferential concentration of particles by turbulence. *Int. J. Multiphase Flow*, 20:169–209, 1994.

[5] S. Balachandar and J. K. Eaton. Turbulent dispersed multiphase flow. *Annu. Rev. Fluid Mech.*, 42:111–133, 2010.

[6] G. C. Truesdell and S. Elghobashi. On the two-way interaction between homogeneous turbulence and dispersed solid particles. II. Particle dispersion. *Phys. Fluids*, 6(3):1405–1407, 1994.

[7] S. Elghobashi. On predicting particle-laden turbulent flows. *Appl. Sci. Res.*, 52(4):309–329, 1994.

[8] J. Capecelatro, O. Desjardins, and R. O. Fox. On fluid–particle dynamics in fully developed cluster-induced turbulence. *J. Fluid Mech.*, 780:578–635, 2015.

[9] B. Kong, R. O. Fox, H. Feng, J. Capecelatro, R. Patel, and O. Desjardins. Euler–Euler anisotropic Gaussian mesoscale simulation of homogeneous cluster-induced gas–particle turbulence. *AIChE J.*, 63(7):2630–2643, 2017.

[10] R. G. Patel, O. Desjardins, B. Kong, J. Capecelatro, and R. O. Fox. Verification of Eulerian–Eulerian and Eulerian–Lagrangian simulations for turbulent fluid–particle flows. *AIChE J.*, 63(12):5396–5412, 2017.

[11] C. D. Dritselis. Direct numerical simulation of particle-laden turbulent channel flows with two- and four-way coupling effects: budgets of Reynolds stress and streamwise enstrophy. *Fluid Dyn. Res.*, 48(1):015507, 2016.

[12] S. Elghobashi. Direct numerical simulation of turbulent flows laden with droplets or bubbles. *Ann. Rev Fluid Mech.*, 51:217–244, 2019.

[13] M. R. Maxey and J. J. Riley. Equation of motion for a small rigid sphere in a nonuniform flow. *Phys. Fluids*, 26(4):883–889, 1983.

[14] R. Gatignol. The Faxén formulae for a rigid particle in an unsteady non-uniform Stokes flow. *Journal de Mécanique Théorique et Appliquée*, 1(2):143–160, 1983.

[15] T. M. Burton and J. K. Eaton. Fully resolved simulations of particle-turbulence interaction. *J. Fluid. Mech.*, 545:67–111, 2005.

[16] M. Uhlmann. Interface-resolved direct numerical simulation of vertical particulate channel flow in the turbulent regime. *Phys. Fluids*, 20(5):053305, 2008.

[17] F. Bianco, S. Chibbaro, C. Marchioli, M. V. Salvetti, and A Soldati. Intrinsic filtering errors of Lagrangian particle tracking in LES flow fields. *Phys. Fluids*, 24(4):045103, 2012.

[18] C. Marchioli, M. V. Salvetti, and A. Soldati. Some issues concerning large-eddy simulation of inertial particle dispersion in turbulent bounded flows. *Phys. Fluids*, 20:040603, 2008.

[19] J. Pozorski and S. V. Apte. Filtered particle tracking in isotropic turbulence and stochastic modeling of subgrid-scale dispersion. *Int. J. Multiphase Flow*, 35(2):118–128, 2009.

[20] E. Peirano, S. Chibbaro, J. Pozorski, and J.-P. Minier. Mean-field/pdf numerical approach for polydispersed turbulent two-phase flows. *Prog. En. Comb. Sci.*, 32(3):315, 2006.

[21] J.-P. Minier. On Lagrangian stochastic methods for turbulent polydisperse two-phase reactive flows. *Prog. En. Comb. Sci.*, 50:1–62, 2015.

[22] A. Innocenti, C. Marchioli, and S. Chibbaro. Lagrangian filtered density function for LES-based stochastic modelling of turbulent particle-laden flows. *Phys. Fluids*, 28(11):115106, 2016.

[23] T. S. Lundgren. Distribution functions in the statistical theory of turbulence. *Phys. Fluids*, 10(5):969–975, 1967.

[24] E. E. O'Brien. Closure approximations applied to stochastically distributed second-order reactants. *Phys. Fluids*, 9(8):1561–1565, 1966.

[25] E. E. O'Brien. Closure for stochastically distributed second-order reactants. *Phys. Fluids*, 11(9):1883–1888, 1968.

[26] E. E. O'Brien. Turbulent mixing of two rapidly reacting chemical species. *Phys. Fluids*, 14(7):1326–1331, 1971.

[27] C. Dopazo and E. E. O'Brien. An approach to the autoignition of a turbulent mixture. *Acta Astronaut.*, 1(9-10):1239–1266, 1974.

[28] E. E. O'Brien. The probability density function (pdf) approach to reacting turbulent flows. In *Turbulent Reacting Flows*, pages 185–218. Springer, Berlin, Heidelberg, New York, 1980.

[29] R. E. Meyers and E. E. O'Brien. The joint pdf of a scalar and its gradient at a point in a turbulent fluid. *Combust. Sci. Technol.*, 26(3-4):123–134, 1981.

[30] E. E. O'Brien. Statistical methods in reacting turbulent flows. *AIAA Journal*, 19(3):366–371, 1981.

[31] S. B. Pope. Pdf methods for turbulent reactive flows. *Prog. En. Comb. Sci.*, 11(2):119–192, 1985.

[32] S. B. Pope. Lagrangian pdf methods for turbulent flows. *Ann. Rev. Fluid Mech.*, 26(1):23–63, 1994.

[33] S. B. Pope. *Turbulent Flows*. Cambridge University Press, Cambridge, UK, 2000.

[34] R. O. Fox. *Computational Models for Turbulent Reacting Flows*. Cambridge Univ Press, Cambridge, UK, 2003.

[35] J.-P. Minier and E. Peirano. The pdf approach to turbulent polydispersed two-phase flows. *Phys. Rep.*, 352:1–214, 2001.

[36] J.-P. Minier, S. Chibbaro, and S. B. Pope. Guidelines for the formulation of Lagrangian stochastic models for particle simulations of single-phase and dispersed two-phase turbulent flows. *Phys. Fluids*, 26(11):113303, 2014.

[37] J.-P. Minier. Statistical descriptions of polydisperse turbulent two-phase flows. *Phys. Rep.*, 665:1–122, 2016.

[38] A. Innocenti, R. O. Fox, M. V. Salvetti, and S. Chibbaro. A Lagrangian probability-density-function model for collisional fluid–particle flows. *J. Fluid. Mech.*, 862:449, 2019.

[39] M. C. Baker, R. O. Fox, B. Kong, J. Capecelatro, and O. Desjardins. Reynolds-stress modeling of clustered-induced turbulence in particle-laden vertical channel flow. *Phys. Rev. Fluids*, 5(7):074304, 2020.

[40] P. Février, O. Simonin, and K. D. Squires. Partitioning of particle velocities in gas–solid turbulent flows into a continuous field and a spatially uncorrelated random distribution: theoretical formalism and numerical study. *J. Fluid Mech.*, 533:1–46, 2005.

[41] R. O. Fox. On multiphase turbulence models for collisional fluid–particle flows. *J. Fluid Mech.*, 742:368–424, 2014.

[42] E. Peirano and J.-P. Minier. Probabilistic formalism and hierarchy of models for polydispersed turbulent two-phase flows. *Phys. Rev. E*, 65:046301, 2002.

[43] J. Capecelatro, O. Desjardins, and R. O. Fox. Strongly coupled fluid–particle flows in vertical channels. II. Turbulence modeling. *Phys. Fluids*, 28(3):033307, 2016.

[44] B. E. Launder, G. Reece Jr., and W. Rodi. Progress in the development of a Reynolds-stress turbulence closure. *J. Fluid Mech.*, 68(03):537–566, 1975.

[45] S. B. Pope. On the relationship between stochastic Lagrangian models of turbulence and second-order closures. *Phys. Fluids*, 6(2):973–985, 1994.

[46] T. D. Dreeben and S. B. Pope. Probability density function and Reynolds-stress modeling of new near-wall turbulent flows. *Phys. Fluids*, 9:154, 1997.

[47] S. Chibbaro and J.-P. Minier. A note on the consistency of hybrid Eulerian/Lagrangian approach to multiphase flows. *Int. J. Multiphase Flow*, 37(3):293–297, 2011.